

# Two Component Dark Matter : A Possible Explanation of 130 GeV $\gamma$ -Ray Line from the Galactic Centre

Anirban Biswas<sup>† 1</sup>, Debasish Majumdar<sup>† 2</sup>, Arunansu Sil<sup>‡ 3</sup>,  
Pijushpani Bhattacharjee<sup>† 4</sup>

<sup>†</sup> *Astroparticle Physics and Cosmology Division,  
Saha Institute of Nuclear Physics, Kolkata 700064, India*

<sup>‡</sup> *Department of Physics, Indian Institute of Technology, Guwahati,  
Guwahati 781039, India*

## ABSTRACT

Recently there has been a hint of a gamma-ray line at 130 GeV originated from the galactic centre after the analysis of the Fermi-LAT satellite data. Being monochromatic in nature, it rules out the possibility of having its astrophysical origin and there has been a speculation that this line could be originated from dark matter annihilation. In this work, we propose a two component dark matter scenario where an extension of the Standard model by an inert Higgs doublet and a gauge singlet scalar concocted with  $Z_2 \times Z'_2$  symmetry, is considered. We find that our scenario can not only explain the 130 GeV gamma-ray line through dark matter annihilation but also produce the correct dark matter relic density. We have used the Standard Model Higgs mass around 125 GeV as intimated by the LHC data.

Keywords : Two component dark matter, Beyond SM, 130 GeV gamma-line

---

<sup>1</sup>email: anirban.biswas@saha.ac.in

<sup>2</sup>email: debasish.majumdar@saha.ac.in

<sup>3</sup>email: sil.arunansu@gmail.com

<sup>4</sup>email: pijush.bhattacharjee@saha.ac.in

# 1 Introduction

Although the existence of dark matter (DM) is now established by various astronomical measurements and observations where the gravitational effects of this huge amount of dark matter is manifested, the particle nature of the dark matter still remains unknown. The particle nature of the dark matter can be probed if it is detected either by direct detection process or by indirect detection. In the former the energy of recoil of a detector nucleus is to be measured if a dark matter indeed scatters off such a nucleus or nucleon. On the other hand the dark matter can be gravitationally trapped inside massive celestial objects such as sun, in regions of galactic centre etc. These trapped dark matter particles eventually annihilate to produce fermion-antifermion pairs or  $\gamma$ s. Study of dark matter through the indirect detection whereby such annihilation products are detected and analyzed, may reveal the nature of the dark matter. Recently it was claimed in Ref. [1] that there is a  $4.6\sigma$  local evidence of a monochromatic gamma-ray line having an energy  $\sim 130$  GeV from the direction of galactic centre, obtained from the analysis of Fermi-LAT publicly available data [2]. Similar result was also followed from the independent analysis of Ref. [3]. Strong evidence for this gamma-ray line from inner galaxy was also reported in Ref. [4] where authors show that this excess of gamma-ray may have a double peak structure with local significance  $5\sigma$  ( $5.4\sigma$ ) for one(two) line(s) case. Later works by [5, 6, 7] indicate the possibility of having double gamma-ray line emission from nearby galaxy clusters and un-associated Fermi-LAT point sources. The analysis of Ref. [8] was also in favour of explaining the galactic centre gamma-ray emission at 130 GeV. There are some other works on this 130 GeV gamma-line which took a critical observation on this line by looking at instrumental noise [9, 10], statistical fluctuations, earth-limb magnification [11] and emission from AGNs [12]. Recently in Ref. [13], authors discuss current observational situation of the 130 GeV gamma-line and propose a new modified survey strategy which increases the data rate from the inner galaxy more than two times of the current standard survey mode for the decisive measurement, by the end of 2014.

A recent search for the spectral lines in the energy range 5-300 GeV using 3.7 years of Fermi-LAT data has been carried out in Ref. [14] by Fermi-LAT collaboration. In this work they have used an updated instrumental calibration. They found that the most significant fit occurred at an energy  $\sim 133$  GeV with a local significance of  $3.3\sigma$ . The other claim was that the line like feature at energy 130 GeV has a weak significance compared to the significance found in earlier analysis. However they also mentioned that at the present situation 133 GeV line can not be considered as a real signal, there may be some other systemic detector effects also. More data and analyses are needed to clarify the origin of this “line-like” gamma-ray feature. In this work, we adopt the 130 GeV gamma-ray line from the galactic centre. We propose a particle physics model for dark matter and attempt to explain this gamma-ray line from such dark matter

annihilation at the galactic centre. However in case the peak indeed exists in the vicinity of 130 GeV, our model can be minimally adjusted to accommodate such deviation.

In the present work we propose a particle physics model for dark matter that can explain the 130 GeV  $\gamma$ -line observed by Fermi-LAT. Our model is in fact a two-component dark matter model in which a real scalar singlet and an inert doublet are added to the Standard Model (SM) of particle physics. There are previous works where either the real scalar singlet model or the inert doublet model has been discussed as one component dark matter model. But, as it will be revealed later that any one of these two models fail to explain individually (as one component dark matter) the observed 130 GeV  $\gamma$ -line from the galactic centre if it is produced due to dark matter annihilation.

In earlier works such as Ref. [15], the authors showed that the scalar dark matter can annihilate into  $\gamma\gamma$  final state with the help of additional charged scalars in a model independent way. It would yield 130 GeV  $\gamma$ s with the required annihilation cross section ( $\langle\sigma v_{\gamma\gamma}\rangle \sim 10^{-27}\text{cm}^3/\text{s}$  given by the analysis [1, 3] of the Fermi-LAT data mentioned above). Different other possibilities involving new particles originated from different extensions of SM have been investigated [16, 17] to explain the 130 GeV  $\gamma$ -line through DM (single candidate) annihilation. However most of these endeavours are restricted in obtaining  $\langle\sigma v_{\gamma\gamma}\rangle \sim 10^{-27}\text{cm}^3/\text{s}$  without going into detailed discussions on relic density calculations, calculation of scattering cross sections relevant for direct detection and their comparisons with experimental (direct detection experiments) or observational (WMAP [18]) results.

One of the simplest choice to accommodate a dark matter is to extend the SM with a gauge singlet real scalar field  $S$  (we will call it real scalar singlet dark matter model, RSDM, from now on) [19, 20, 21], which couples to SM Higgs ( $h$ ). The use of a  $Z_2$  symmetry ensures the stability of the dark matter candidate. In Ref. [21] it is shown that this type of model fails to explain the 130 GeV gamma-ray line from the Galactic centre. The reason of this failure is related with the relatively small annihilation cross section of two  $S$  fields into two  $\gamma$ s considering the fact that  $S$  should contribute to the correct amount of relic density as predicted by WMAP data [18]. In [20], it was shown that with SM Higgs much heavier than 125 GeV could in principle lead to  $\langle\sigma v_{\gamma\gamma}\rangle \sim 10^{-27}\text{cm}^3/\text{s}$  with  $m_S \sim 130$  GeV, when the constraint on the  $S$  field to produce right amount of dark matter abundance is relaxed. However once this constraint is applied, the  $\langle\sigma v_{\gamma\gamma}\rangle$  becomes few orders of magnitude less than required. In addition to these findings, if we employ the recent constraint on the Higgs mass from LHC experiment [22] on the SM Higgs, then we infer that strictly within RSDM picture, we can not accommodate both the relic density as well as the 130 GeV  $\gamma$ -line from DM annihilation.

Another well motivated dark matter model is the inert doublet model (IDM) [23, 24, 25] which requires an extension of the SM by a scalar Higgs (inert) doublet  $\Phi$  having a  $Z_2$ . In Ref.

[24], it was shown that there exists an allowed region (consistent with the WMAP results of relic density) in IDM for dark matter<sup>5</sup>  $\phi^0$  having mass in the range between 80 GeV and 160 GeV provided the mass of the dark matter candidate ( $m_{\phi^0}$ ) is less than the mass of SM Higgs (and top quark),  $m_{\phi^0} < m_{h,t}$ . This condition was imposed to reduce the  $\langle\sigma v\rangle_{\text{total}}$  (to get rid of the contributions like  $\phi^0\phi^0 \rightarrow hh$  (and/or  $tt$ )) since otherwise the relic density would be small<sup>6</sup>. Then they found that due to accidental cancellations of different Feynman diagrams for annihilation into gauge bosons,  $\langle\sigma v\rangle_{\text{total}}$  can indeed be the right amount for a judicious choice of parameter space involved in the model.

We are trying to find a resolution where a right amount of dark matter relic density could be obtained as well as an explanation of the 130 GeV gamma-ray line of Fermi-LAT can also be probed through DM annihilation. Now with the consideration that the SM Higgs boson has a mass  $m_h \sim 125$  GeV [22] and mass of the DM candidate 130 GeV (in order to explain the 130 GeV gamma-ray line from Fermi-LAT, the mass of the DM should be in this range), the above mentioned condition  $m_{\phi^0} < m_{h,t}$  related to the IDM is evaded thereby the channel of annihilation,  $\phi^0\phi^0 \rightarrow hh$ , opens up. Hence  $\langle\sigma v\rangle_{\text{total}}$  will increase and the final relic density in this sort of model [24] can accommodate only (10-30)% of the observed DM relic density [18]. However this result has an interesting consequence. We can compensate this deficit of the DM relic density by another candidate of DM while  $\phi^0$  explains the 130 GeV gamma-line through its annihilation.

Keeping in mind the above mentioned scenarios (particularly the RSDM and IDM), we propose that the dark matter can actually be composed of two fields, namely a scalar singlet ( $S$ ) and an inert doublet ( $\Phi$ ). The additional feature of this model would be that these two components possess an interaction between them via a term like  $(\Phi^\dagger\Phi)SS$ . The 130 GeV  $\gamma$ -line will be produced by the annihilation of the component  $\phi^0$  while the role of other component  $S$ , besides contributing to the overall relic density is to increase  $\phi^0$  contribution to the combined relic density through  $(\Phi^\dagger\Phi)SS$ . A model with a scalar singlet and a doublet was presented in [26, 27] in the context of GUT models. A multi-component dark matter was proposed in [28] earlier where an additional fermion singlet and a scalar singlet were introduced, though not in the context of the possibility of having 130 GeV gamma-ray from DM annihilation. We have imposed a discrete  $Z_2 \times Z'_2$ , under which  $S$  and  $\Phi$  transform non-trivially.

The calculation of the flux for 130 GeV  $\gamma$ -ray from galactic centre region also requires the knowledge of dark matter density in the region of the galactic centre. In the absence of a unique density profile in literature we consider in the present work two dark matter density profiles namely NFW (Navarro-Frenk-White) profile [29] and Einasto profile [30] and compute the flux

---

<sup>5</sup> $\phi^0$  is the neutral component of the extra Higgs doublet.

<sup>6</sup>since relic density  $\Omega h^2 \propto 1/\langle\sigma v\rangle$ .

using the cross section  $\langle\sigma v_{\phi^0\phi^0\rightarrow\gamma\gamma}\rangle$  calculated in this work from our model.

The paper is arranged as follows. In Section 2 we describe the structure of our two component dark matter model. Section 3 discusses the calculations of the relic densities of each dark matter components and hence the combined relic density by simultaneously solving the two Boltzmann's equations for the two components. In Section 4 we discuss how to constrain the parameter space of the model by comparing the relic density results with WMAP and the scattering cross section results with the direct detection experiments data. Section 5 gives the cross section calculations for 130 GeV  $\gamma$ -ray from  $\phi^0\phi^0$  annihilation and hence the calculations of  $\gamma$ -ray flux using different dark matter halo models. Finally in Section 6 we present some discussions and conclusions.

## 2 The Two Component Dark Matter Model

In the present work, the DM sector is composed of a real gauge singlet scalar field,  $S$  and an extra (in addition to the usual Higgs doublet,  $H$ ) scalar doublet field,  $\Phi$  (doublet under  $SU(2)_L$ ). An exact (unbroken) discrete symmetry  $Z_2 \times Z'_2$  is imposed under which all the SM particles are even, i.e. having  $Z_2 \times Z'_2$  charge as (1,1) and for  $\Phi$ ,  $S$  the  $Z_2 \times Z'_2$  charges are (1,-1) and (-1,1) respectively. Thereby both  $S$  and  $\Phi$  are fermiophobic and do not develop any vacuum expectation value (VEV) and hence inert. The construction therefore ensures the stability of both  $S$  and  $\Phi$  in this two component dark matter scenario. The scalar doublet  $\Phi$  can be written as

$$\Phi = \begin{pmatrix} \phi^+ \\ \frac{\phi^0 + iA^0}{\sqrt{2}} \end{pmatrix}. \quad (1)$$

The Lagrangian of the construction can be read as,  $\mathcal{L} = \mathcal{L}_{\text{SM}} + \mathcal{L}_{\text{DM}}$ , where  $\mathcal{L}_{\text{SM}}$  is the Standard Model Lagrangian and  $\mathcal{L}_{\text{DM}}$  stands for the DM sector consistent with all the symmetries.  $\mathcal{L}_{\text{DM}}$  is then given by,

$$\mathcal{L}_{\text{DM}} = \mathcal{L}_{\text{RSDM}} + \mathcal{L}_{\text{IDM}} + \mathcal{L}_{\text{INT}}, \quad (2)$$

where  $\mathcal{L}_{\text{RSDM}}$  and  $\mathcal{L}_{\text{IDM}}$  refer to the individual Lagrangian of real singlet scalar and inert doublet dark matter respectively and  $\mathcal{L}_{\text{INT}}$  is the additional part representing the interaction between the two components of DM. So the most general form of them, consistent with the SM gauge group as well as the discrete symmetry imposed, is as follows,

$$\mathcal{L}_{\text{RSDM}} = \frac{1}{2}\partial_\mu S \partial^\mu S - \frac{\kappa_1^2}{2}S^2 - \frac{\kappa_2}{4}S^4 - \lambda_6(H^\dagger H)SS, \quad (3)$$

$$\begin{aligned} \mathcal{L}_{\text{IDM}} = & (D_\mu \Phi)^\dagger (D^\mu \Phi) - \mu_2^2(\Phi^\dagger \Phi) - \rho_2(\Phi^\dagger \Phi)^2 - \lambda_1(H^\dagger H)(\Phi^\dagger \Phi) - \\ & \lambda_2(\Phi^\dagger H)(H^\dagger \Phi) - \lambda_3 [(\Phi^\dagger H)^2 + h.c], \end{aligned} \quad (4)$$

$$\mathcal{L}_{\text{INT}} = -\lambda_5 (\Phi^\dagger \Phi) SS. \quad (5)$$

The SM Higgs Lagrangian is included in the  $\mathcal{L}_{\text{SM}}$ . In this model we have five new particles, two charged scalar ( $\phi^\pm$ ) and three neutral scalar particles ( $\phi^0$ ,  $S$ ,  $A^0$ ). Due to the stability and electrical charge neutrality we consider  $\phi^0$  and  $S$  as two viable components of dark matter in this model.

After spontaneous breaking of the SM gauge symmetry, the masses of these new particles and Higgs are given by,

$$m_{\phi^\pm}^2 = \mu_2^2 + \frac{1}{2}\lambda_1 v^2, \quad (6)$$

$$m_{\phi^0}^2 = \mu_2^2 + \alpha v^2, \quad (7)$$

$$m_{A^0}^2 = \mu_2^2 + \beta v^2, \quad (8)$$

$$m_S^2 = \kappa_1^2 + \lambda_6 v^2, \quad (9)$$

$$m_h^2 = 2\rho_1 v^2, \quad (10)$$

where  $v$  ( $= 246$  GeV) is the Higgs VEV and  $\rho_1$  is the coefficient of the quartic coupling of the SM Higgs (part of  $\mathcal{L}_{\text{SM}}$  here) potential. The parameters  $\alpha$  and  $\beta$  are defined in terms of  $\lambda$ 's as

$$\begin{aligned} \alpha &= \frac{1}{2}(\lambda_1 + \lambda_2 + 2\lambda_3), \\ \beta &= \frac{1}{2}(\lambda_1 + \lambda_2 - 2\lambda_3). \end{aligned} \quad (11)$$

As is evident from the above set up, the model involves 10 parameters in total, specifically  $m_h$ ,  $m_{\phi^0}$ ,  $m_{A^0}$ ,  $m_{\phi^\pm}$ ,  $m_S$ ,  $\alpha$ ,  $\lambda_5$ ,  $\lambda_6$ ,  $\kappa_2$ ,  $\rho_2$ . Now fixing the Higgs mass  $m_h$  at 125 GeV, we have altogether 9 parameters, which are further restricted from theoretical bounds as well as from experimental results as discussed below.

- **Vacuum Stability** - The Lagrangian of this model (Eq. (2)) must be bounded from below. This condition will be satisfied if

$$\rho_1, \rho_2, \kappa_2 > 0, \quad (12)$$

$$\alpha, \beta > -\sqrt{\rho_1 \rho_2}, \quad (13)$$

$$\lambda_1 > -2\sqrt{\rho_1 \rho_2}, \quad (14)$$

$$\lambda_6 > -\sqrt{\rho_1 \kappa_2}, \quad (15)$$

$$\lambda_5 > -\sqrt{\rho_2 \kappa_2}. \quad (16)$$

- **Zero VEV of  $\Phi$  and  $S$**  - Ground state of the Lagrangian Eq. (2) must preserve  $Z_2 \times Z_2'$  symmetry for stability of the dark matter candidates, this leads to the condition that the VEV of both  $\Phi$ ,  $S$  is zero.

- **Perturbativity**- In order to be within the perturbative limit, the model parameters cannot be too large. This can be ensured provided

$$|\text{model parameters}| < 4\pi. \quad (17)$$

- **Neutral Scalar Mass** - The LEP [31] measurement of the  $Z$  boson decay width leads to the condition

$$m_{A^0} + m_{\phi^0} > m_Z. \quad (18)$$

- **WMAP Limit** - The Combined relic density of the dark matter components must satisfy the WMAP limit [18],

$$0.1053 < \Omega_{\text{DM}} h^2 < 0.1165 \text{ at } 68\% \text{ C.L.} \quad (19)$$

for the dark matter in the Universe. This condition will further constrain the parameter space of this model discussed above.

- **Direct detection limits of dark matter** - The results of the ongoing experiments for direct detection of dark matter also impose additional limits on the relevant parameters of the present two component dark matter model. Being inert, the elastic scattering between

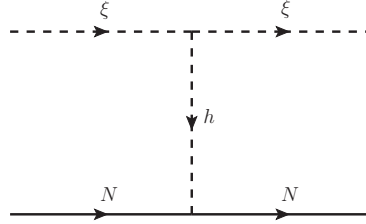


Figure 1: Feynman diagram for the elastic scattering between dark matter particle  $\xi$  (i.e.  $S, \phi^0$ ) and nucleon  $N$  of the detector material via Higgs exchange.

the dark matter candidate  $\xi$  (here  $\phi^0$  and/or  $S$ ) and nucleons ( $N$ ) can take place only with the SM Higgs exchange as in Fig 1. The relevant term in the Lagrangian which describes the interaction between  $\xi$  and Higgs is given by

$$\mathcal{L} = -k\xi^2 h, \quad (20)$$

where the coupling  $k = \alpha v$  ( $\lambda_6 v$ ) for  $\xi = \phi^0$  ( $S$ ). The spin independent scattering cross section for this process,  $\xi N \rightarrow \xi N$ , is given by [32],

$$\sigma^{\text{SI}} = \frac{f^2}{\pi} \left( \frac{k}{v} \right)^2 \frac{\mu^2 m_N^2}{m_\xi^2 m_h^4}, \quad (21)$$

where  $m_\xi$  and  $m_N$  are the masses of the DM candidate and nucleons respectively,  $\mu = \frac{m_\xi m_N}{m_\xi + m_N}$  is the reduced mass and  $f$  represents the strength of the effective interaction which depends upon the number of heavy quarks involved [33]. In this work, we have considered the value of  $f = 0.3$  [25, 34].

An upper limit on  $\sigma^{\text{SI}}$  for a particular mass of dark matter particle would automatically sets an upper bound on the absolute value of the couplings  $\alpha$  and  $\lambda_6$  through Eq. (21) (note that we are considering a two-component DM case). Now to find out this limit, we need to know the masses of our DM candidates, which should not only explain the correct DM relic abundance, but also can explain the 130 GeV gamma-line obtained from Fermi-LAT data. It is discussed in the rest of our paper and we infer that both masses should be similar and  $\sim 130$  GeV. With this two-component DM model, the direct detection limit implies [28],

$$\epsilon_{\phi^0} \sigma_{\phi^0 N} + \epsilon_S \sigma_{SN} < \sigma_0, \quad (22)$$

where  $\sigma_0$  is the upper limit of the DM-nucleon scattering cross section (for one dark matter model) obtained from the direct search experiment. In case of XENON 100 (2012) [35], it is  $3 \times 10^{-45} \text{ cm}^2$  at 90% C.L. Using Eq.(21), it then translates into the following inequality,

$$\epsilon_{\phi^0} \alpha^2 + \epsilon_S \lambda_6^2 < (0.038)^2, \quad (23)$$

where  $\epsilon_{\phi^0, S} = \frac{\Omega_{\phi^0, S} h^2}{\Omega_c h^2}$ . Here  $\Omega_i h^2$  corresponds to the relic density of the  $i$ th type DM relic and  $\Omega_c h^2$  is the total relic density of DM in the universe (see Eq. (30)).

### 3 Combined Relic Density Calculation for the two dark matter Candidates $\phi^0$ and $S$

In the present two component dark matter model, the total relic density of the dark matter in the universe will have contributions from both the components  $S$  and  $\phi^0$ . While both are annihilating into the SM particles, the heavier component,  $S$  can annihilate into the lighter component,  $\phi^0$  too. In order to obtain the correct combined relic density we have to solve Boltzmann's equation for each components simultaneously. The coupled Boltzmann's equations [36] to study the evolution of the number densities of the two dark matter candidates ( $n_S$  and  $n_{\phi^0}$ ) are given by,

$$\frac{dn_S}{dt} + 3n_S H = -\langle \sigma v_{SS \rightarrow \chi\bar{\chi}} \rangle (n_S^2 - (n_S^{eq})^2) - \langle \sigma v_{SS \rightarrow \phi^0 \phi^0} \rangle \left( n_S^2 - \frac{(n_S^{eq})^2}{(n_{\phi^0}^{eq})^2} n_{\phi^0}^2 \right), \quad (24)$$



$$\frac{dn_{\phi^0}}{dt} + 3n_{\phi^0}H = -\langle\sigma v_{\phi^0\phi^0\rightarrow\chi\bar{\chi}}\rangle\left(n_{\phi^0}^2 - (n_{\phi^0}^{eq})^2\right) + \langle\sigma v_{SS\rightarrow\phi^0\phi^0}\rangle\left(n_S^2 - \frac{(n_S^{eq})^2}{(n_{\phi^0}^{eq})^2}n_{\phi^0}^2\right). \quad (25)$$

Here  $n_{\phi^0}^{eq}$  and  $n_S^{eq}$  are the equilibrium values of  $n_{\phi^0}$  and  $n_S$  respectively,  $H$  is the Hubble's constant.  $\chi$  represents any SM particle such as leptons, quarks, gauge bosons, Higgs boson. The annihilation of  $SS$  into  $\phi^0\phi^0$  is included through the annihilation cross section  $\langle\sigma v_{SS\rightarrow\phi^0\phi^0}\rangle$ , the expression of which in our scenario is discussed later in this section explicitly along with the total annihilation cross section. The possible inclusion of co-annihilation terms for the channels  $\phi^0\phi^\pm \rightarrow \chi\chi'$  and  $\phi^0 A^0 \rightarrow \chi\chi'$  will be discussed later.

Introducing two dimensionless variables  $Y_i = \frac{n_i}{s}$  and  $x_i = \frac{m_i}{T}$  with  $i = S, \phi^0$ , where  $s$  and  $T$  are the entropy density and temperature of the universe respectively, Eqs. (24, 25) can be written as

$$\frac{dY_S}{dx_S} = -\left(\frac{45G}{\pi}\right)^{-\frac{1}{2}} \frac{m_S}{x_S^2} \sqrt{g_\star} \left( \langle\sigma v_{SS\rightarrow\chi\bar{\chi}}\rangle (Y_S^2 - (Y_S^{eq})^2) + \langle\sigma v_{SS\rightarrow\phi^0\phi^0}\rangle \left( Y_S^2 - \frac{(Y_S^{eq})^2}{(Y_{\phi^0}^{eq})^2} Y_{\phi^0}^2 \right) \right), \quad (26)$$

$$\frac{dY_{\phi^0}}{dx_{\phi^0}} = -\left(\frac{45G}{\pi}\right)^{-\frac{1}{2}} \frac{m_{\phi^0}}{x_{\phi^0}^2} \sqrt{g_\star} \left( \langle\sigma v_{\phi^0\phi^0\rightarrow\chi\bar{\chi}}\rangle (Y_{\phi^0}^2 - (Y_{\phi^0}^{eq})^2) - \langle\sigma v_{SS\rightarrow\phi^0\phi^0}\rangle \left( Y_S^2 - \frac{(Y_S^{eq})^2}{(Y_{\phi^0}^{eq})^2} Y_{\phi^0}^2 \right) \right). \quad (27)$$

Here  $G$  is the Gravitation constant and  $g_\star$  is defined as,

$$\sqrt{g_\star} = \frac{h_{\text{eff}}(T)}{\sqrt{g_{\text{eff}}(T)}} \left( 1 + \frac{1}{3} \frac{d \ln(h_{\text{eff}}(T))}{d \ln(T)} \right), \quad (28)$$

with  $g_{\text{eff}}(T)$  and  $h_{\text{eff}}(T)$  are the effective degrees of freedom related to the energy and entropy densities through  $\rho = g_{\text{eff}}(T) \frac{\pi^2}{30} T^4$ ,  $s = h_{\text{eff}}(T) \frac{2\pi^2}{45} T^3$ .

Once we get the values of  $Y_{\phi^0}$  and  $Y_S$  at the present temperature  $T_0$  after solving the coupled Eqs. (26, 27), we will be able to calculate the individual contributions  $\Omega_{\phi^0}$  and  $\Omega_S$  from [37],

$$\Omega_i h^2 = 2.755 \times 10^8 \left( \frac{m_i}{\text{GeV}} \right) Y_i(T_0), \quad (29)$$

(using the present values of  $s$  and  $h$ ). In this work we have solved the coupled Boltzmann equations numerically to get the values of  $Y_i(T_0)$ . After having these estimates, the total relic density of the universe can be obtained through

$$\Omega_c h^2 = \Omega_{\phi^0} h^2 + \Omega_S h^2. \quad (30)$$

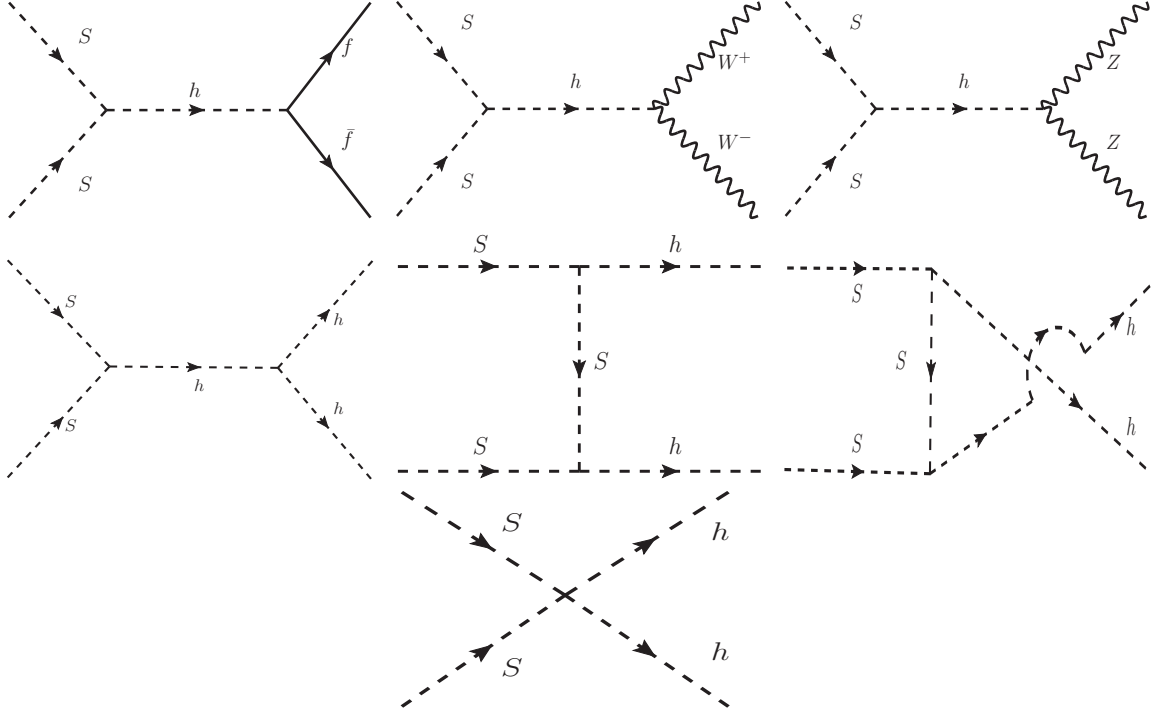


Figure 2: Lowest order Feynman diagrams of two  $S$  annihilate into a pair of fermion and anti-fermion,  $W^+W^-$ ,  $ZZ$  and Higgs.

As we mentioned before,  $\langle\sigma v_{SS\rightarrow\chi\bar{\chi}}\rangle$  in Eq.(24) represents the total annihilation cross section of two  $S$  particles into SM particles such as leptons and quarks ( $f\bar{f}$ ), gauge bosons ( $W^+W^-$ ,  $ZZ$ ) and Higgs boson ( $h$ ). The Feynman diagrams for all the processes are shown in Fig. 2. The expressions of annihilation cross sections of two  $S$  particles for these final states are given below [38].

$$\langle\sigma v_{SS\rightarrow f\bar{f}}\rangle = \left(\frac{g_{SSh}}{v}\right)^2 \frac{m_f^2}{\pi} \frac{\left(1 - \frac{m_f^2}{m_S^2}\right)^{3/2}}{[(4m_S^2 - m_h^2)^2 + (\Gamma_h m_h)^2]}, \quad (31)$$

$$\langle\sigma v_{SS\rightarrow W^+W^-}\rangle = 2 \left(\frac{g_{SSh}}{v}\right)^2 \frac{m_S^2}{\pi} \frac{\left(1 - \frac{m_W^2}{m_S^2}\right)^{1/2}}{[(4m_S^2 - m_h^2)^2 + (\Gamma_h m_h)^2]} \left(1 - \frac{m_W^2}{m_S^2} + \frac{3}{4} \frac{m_W^4}{m_S^4}\right), \quad (32)$$

$$\langle\sigma v_{SS\rightarrow ZZ}\rangle = \left(\frac{g_{SSh}}{v}\right)^2 \frac{m_S^2}{\pi} \frac{\left(1 - \frac{m_Z^2}{m_S^2}\right)^{1/2}}{[(4m_S^2 - m_h^2)^2 + (\Gamma_h m_h)^2]} \left(1 - \frac{m_Z^2}{m_S^2} + \frac{3}{4} \frac{m_Z^4}{m_S^4}\right), \quad (33)$$

$$\langle\sigma v_{SS\rightarrow hh}\rangle = \frac{1}{4\pi m_S^2} \left(1 - \frac{m_h^2}{m_S^2}\right)^{1/2} \left[ \left( \frac{3 g_{SSh} m_h^2}{2v(4m_S^2 - m_h^2)} \right)^2 + \frac{3 g_{SSh} g_{SShh} m_h^2}{v(4m_S^2 - m_h^2)} \right]$$

Interactions involving $XYZ(P)$	$g_{xyz(p)}$
$SSh$	$g_{SSh} = -\lambda_6 v$
$SShh$	$g_{SShh} = -\frac{1}{2}\lambda_6$
$\phi^0\phi^0h$	$g_{\phi^0\phi^0h} = -\alpha v$
$\phi^0\phi^0hh$	$g_{\phi^0\phi^0hh} = -\frac{1}{2}\alpha$
$\phi^0\phi^0W^+W^-$	$g_{\phi^0\phi^0W^+W^-} = \frac{m_W^2}{v^2}$
$\phi^0\phi^0ZZ$	$g_{\phi^0\phi^0ZZ} = \frac{m_Z^2}{2v^2}$
$\phi^0\phi^0\phi^+\phi^-$	$g_{\phi^0\phi^0\phi^+\phi^-} = -\rho_2$
$SS\phi^0\phi^0$	$-\frac{1}{2}\lambda_5$

Table 1: Interactions and the corresponding couplings.

$$\begin{aligned}
& +g_{SShh}^2 + \frac{4 g_{SSh}^2 g_{SShh}}{2m_S^2 - m_h^2} + \frac{6 g_{SSh}^3 m_h^2}{v(2m_S^2 - m_h^2)(4m_S^2 - m_h^2)} \\
& + \left( \frac{2 g_{SSh}^2}{2m_S^2 - m_h^2} \right)^2 \Big]. \tag{34}
\end{aligned}$$

In writing the expression for the cross sections, we have introduced the notation  $g_{xyz}$  (or  $g_{xyzp}$ ) which are related to the coupling constants of the corresponding interaction Lagrangian through  $\mathcal{L} = g_{xyz}XYZ$  (or  $\mathcal{L} = g_{xyzp}XYZP$ ). Here  $X, Y, Z, P$  are the fields involved in a particular process. All the  $g_{XYZ}$  and  $g_{XYZP}$  are listed in Table 1. The masses for fermion  $f$ ,  $W$  boson,  $Z$  boson and Higgs boson are denoted by  $m_f, m_W, m_Z, m_h$  respectively and  $\Gamma_h$  represents the Higgs decay width.

Similarly in Eq. (25),  $\langle \sigma v_{\phi^0\phi^0 \rightarrow \chi\bar{\chi}} \rangle$  represents the total annihilation cross section of two  $\phi^0$  particles into SM particles. The Feynman diagrams of individual processes are shown in Fig. 3 and the expressions of annihilation cross sections for these channels are given below.

$$\begin{aligned}
\langle \sigma v_{\phi^0\phi^0 \rightarrow f\bar{f}} \rangle &= \left( \frac{g_{\phi^0\phi^0h}}{v} \right)^2 \frac{m_f^2}{\pi} \frac{\left( 1 - \frac{m_f^2}{m_{\phi^0}^2} \right)^{3/2}}{\left[ (4m_{\phi^0}^2 - m_h^2)^2 + (\Gamma_h m_h)^2 \right]}, \tag{35} \\
\langle \sigma v_{\phi^0\phi^0 \rightarrow W^+W^-} \rangle &= \frac{1}{2\pi} \left( 1 - \frac{m_W^2}{m_{\phi^0}^2} \right)^{1/2} \left[ m_{\phi^0}^2 \left( 1 - \frac{m_W^2}{m_{\phi^0}^2} + \frac{3m_W^4}{4m_{\phi^0}^4} \right) \left\{ \left( \frac{g_{\phi^0\phi^0W^+W^-}}{m_W^2} \right)^2 + \right. \right. \\
&\quad \left. \left. \frac{\left( \frac{2 g_{\phi^0\phi^0h}}{v} \right)^2}{\left[ (4m_{\phi^0}^2 - m_h^2)^2 + (\Gamma_h m_h)^2 \right]} - \frac{\left( \frac{4 g_{\phi^0\phi^0h}}{m_W^2 v} \frac{g_{\phi^0\phi^0W^+W^-}}{m_W^2 v} \right) (4m_{\phi^0}^2 - m_h^2)}{\left[ (4m_{\phi^0}^2 - m_h^2)^2 + (\Gamma_h m_h)^2 \right]} \right\} \right]
\end{aligned}$$

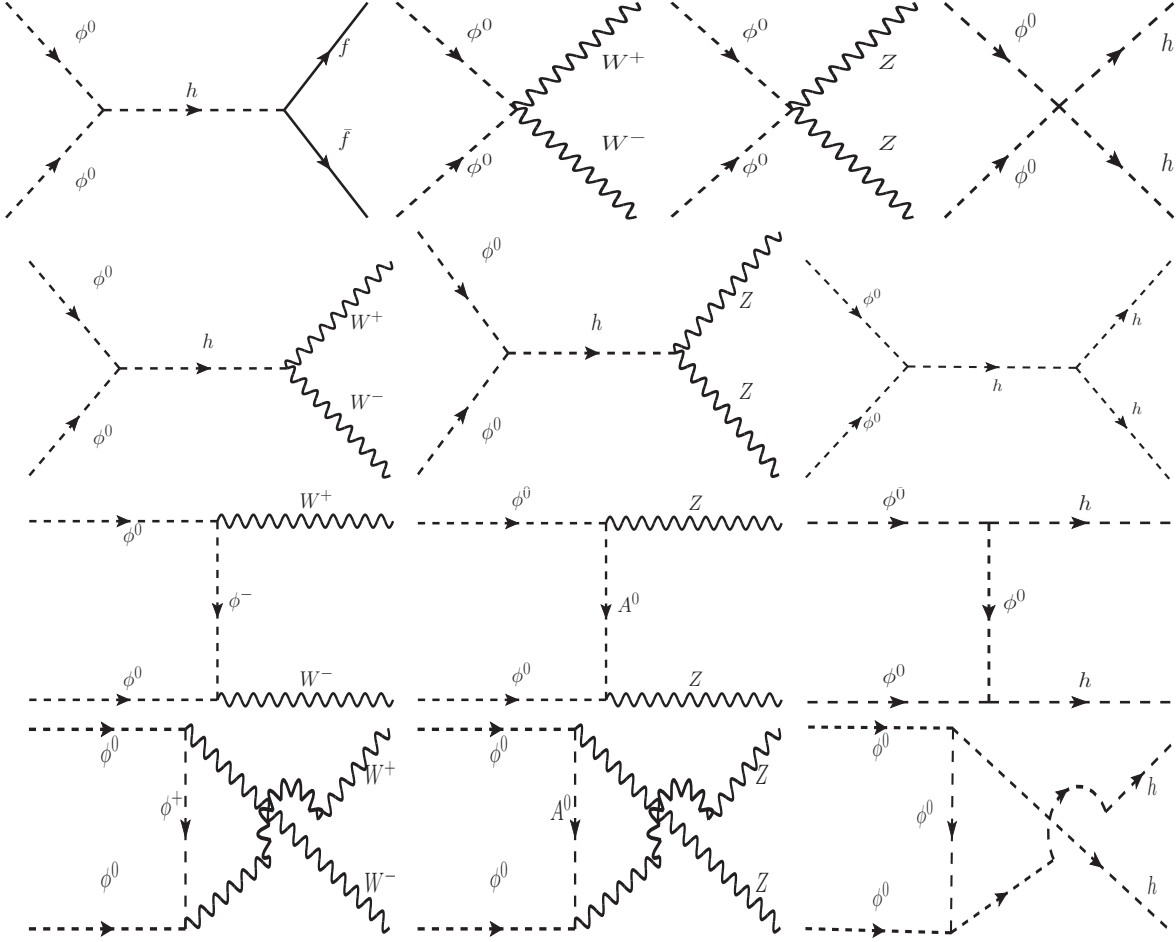


Figure 3: Lowest order Feynman diagrams of two  $\phi^0$  annihilate into a pair of fermion and anti-fermion,  $W^+W^-$ ,  $ZZ$  and Higgs.

$$\begin{aligned}
& + \frac{g^2}{4} \left\{ \left( g_{\phi^0\phi^0 W^+W^-} - \frac{2 g_{\phi^0\phi^0 h} (4m_{\phi^0}^2 - m_h^2) m_W^2}{v [(4m_{\phi^0}^2 - m_h^2)^2 + (\Gamma_h m_h)^2]} \right) \times \right. \\
& 2 \left( \frac{(m_W^4 - 3m_W^2 m_{\phi^0}^2 + 2m_{\phi^0}^4)}{m_W^4 (m_W^2 - m_{\phi^+}^2 - m_{\phi^0}^2)} \right) \\
& \left. + g^2 \left( \frac{m_{\phi^0} (m_W^2 - m_{\phi^0}^2)}{m_W^2 (m_{\phi^+}^2 - m_W^2 + m_{\phi^0}^2)} \right)^2 \right\} , \\
& \langle \sigma v_{\phi^0\phi^0 \rightarrow ZZ} \rangle = \frac{1}{4\pi} \left( 1 - \frac{m_Z^2}{m_{\phi^0}^2} \right)^{1/2} \left[ m_{\phi^0}^2 \left( 1 - \frac{m_Z^2}{m_{\phi^0}^2} + \frac{3m_Z^4}{4m_{\phi^0}^4} \right) \left\{ \left( \frac{2 g_{\phi^0\phi^0 ZZ}}{m_Z^2} \right)^2 + \right. \right. \\
& \left. \left. \left( \frac{2 g_{\phi^0\phi^0 h}}{m_h^2} \right)^2 + \left( \frac{2 g_{\phi^0\phi^0 W^+W^-}}{m_W^2} \right)^2 \right\} \right] ,
\end{aligned} \tag{36}$$

$$\begin{aligned}
& \left\{ \frac{\left( \frac{2 g_{\phi^0 \phi^0 h}}{v} \right)^2}{\left[ (4m_{\phi^0}^2 - m_h^2)^2 + (\Gamma_h m_h)^2 \right]} - \frac{\left( \frac{8 g_{\phi^0 \phi^0 h} g_{\phi^0 \phi^0 ZZ}}{m_Z^2 v} \right) (4m_{\phi^0}^2 - m_h^2)}{\left[ (4m_{\phi^0}^2 - m_h^2)^2 + (\Gamma_h m_h)^2 \right]} \right\} \\
& + \frac{g^2}{4 \cos^2 \theta_W} \left\{ 2 \left( \frac{(m_Z^4 - 3m_Z^2 m_{\phi^0}^2 + 2m_{\phi^0}^4)}{m_Z^4 (m_Z^2 - m_{A^0}^2 - m_{\phi^0}^2)} \right) \right. \\
& \times \left( 2 g_{\phi^0 \phi^0 ZZ} - \frac{2 g_{\phi^0 \phi^0 h} (4m_{\phi^0}^2 - m_h^2) m_Z^2}{v \left[ (4m_{\phi^0}^2 - m_h^2)^2 + (\Gamma_h m_h)^2 \right]} \right) \\
& \left. + \frac{g^2}{\cos^2 \theta_W} \left( \frac{m_{\phi^0} (m_Z^2 - m_{\phi^0}^2)}{m_Z^2 (m_{A^0}^2 - m_Z^2 + m_{\phi^0}^2)} \right)^2 \right\} , \tag{37}
\end{aligned}$$

$$\begin{aligned}
\langle \sigma v_{\phi^0 \phi^0 \rightarrow hh} \rangle &= \frac{1}{4\pi m_{\phi^0}^2} \left( 1 - \frac{m_h^2}{m_{\phi^0}^2} \right)^{1/2} \left[ \left( \frac{3 g_{\phi^0 \phi^0 h} m_h^2}{2v(4m_{\phi^0}^2 - m_h^2)} \right)^2 + g_{\phi^0 \phi^0 hh}^2 \right. \\
& + \frac{3 g_{\phi^0 \phi^0 h} g_{\phi^0 \phi^0 hh} m_h^2}{v(4m_{\phi^0}^2 - m_h^2)} + \left( \frac{2 g_{\phi^0 \phi^0 h}^2}{2m_{\phi^0}^2 - m_h^2} \right)^2 + \frac{4 g_{\phi^0 \phi^0 h}^2 g_{\phi^0 \phi^0 hh}}{2m_{\phi^0}^2 - m_h^2} \\
& \left. + \frac{6 g_{\phi^0 \phi^0 h}^3 m_h^2}{v(2m_{\phi^0}^2 - m_h^2)(4m_{\phi^0}^2 - m_h^2)} \right] . \tag{38}
\end{aligned}$$

The other cross section involved in the coupled Boltzmann equations is  $\langle \sigma v_{SS \rightarrow \phi^0 \phi^0} \rangle$  (due to the presence of the interaction between the two dark matter components  $S$  and  $\phi^0$ ). The expression for this cross section is given by

$$\begin{aligned}
\langle \sigma v_{SS \rightarrow \phi^0 \phi^0} \rangle &= \frac{1}{4\pi m_S^2} \left( 1 - \frac{m_{\phi^0}^2}{m_S^2} \right)^{1/2} \left[ \frac{(g_{\phi^0 \phi^0 h} g_{SSh})^2}{\left[ (4m_S^2 - m_h^2)^2 + (\Gamma_h m_h)^2 \right]} + g_{\phi^0 \phi^0 SS}^2 \right. \\
& \left. - \frac{(2 g_{\phi^0 \phi^0 h} g_{SSh} g_{\phi^0 \phi^0 SS}) (4m_S^2 - m_h^2)}{\left[ (4m_S^2 - m_h^2)^2 + (\Gamma_h m_h)^2 \right]} \right] . \tag{39}
\end{aligned}$$

The heavier component of DM is chosen to be  $S$  in our case<sup>7</sup>. Since only  $\phi^0$  will contribute to the 130 GeV gamma-ray production (the annihilation cross section  $\langle \sigma v_{SS \rightarrow \gamma \gamma} \rangle$  for the singlet  $S$  is not enough to produce Fermi-LAT observed 130 GeV  $\gamma$ -ray flux as we argued before), its mass should be  $m_{\phi^0} \sim 130$  GeV. We will show later that  $\phi^0$  with its mass  $\sim 130$  GeV can not accommodate the total relic density consistent with the WMAP data. So the rest of the relic density should be provided by the other component  $S$ . And we find that it would be a good choice

---

<sup>7</sup>If  $m_S < m_{\phi^0}$ ,  $\phi^0$  component would be annihilated into  $S$  (via the process  $\phi^0 \phi^0 \rightarrow SS$ ). This would reduce the contribution of  $\phi^0$  to the combined relic density and hence the  $\gamma$ -ray flux originated from  $\phi^0 \phi^0$  annihilation would be suppressed.

to make  $m_S > m_{\phi^0}$ . The involvement of this interaction between two dark matter components is a salient feature of our analysis. It would enhance the number density of  $\phi^0$  through the annihilation of  $SS$  during evolution. The Feynman diagrams for this process ( $SS \rightarrow \phi^0\phi^0$ ) are given in Fig. 4.

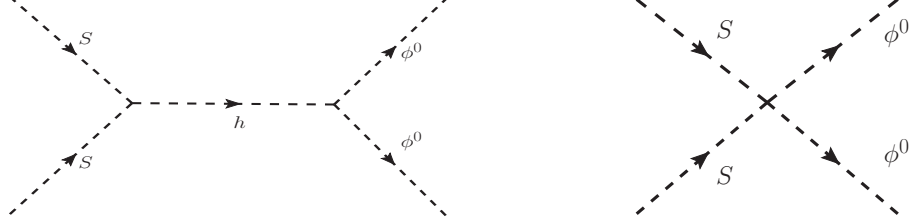


Figure 4: Feynman diagrams for the annihilation channel  $SS \rightarrow \phi^0\phi^0$

Note that the relic density of the component  $\phi^0$  also depends on its co-annihilation with the charged scalars  $\phi^\pm$  and CP odd neutral scalar  $A^0$ . As the present scenario demands  $m_{\phi^\pm} \gtrsim m_{\phi^0}$  and  $m_{A^0} \gg m_{\phi^0}$  for the explanation of 130 GeV gamma-line and the exclusion of charged relic in the model simultaneously (see Section 4 and 5 for more discussion on this topic), the effect of co-annihilation term between  $\phi^0$  and  $\phi^\pm$  could have a significant contribution compared to the other term between  $\phi^0$  and  $A^0$  [37, 39]. Therefore the Boltzmann's Equation (Eq. (24)) for  $\phi^0$  should have another term describing the co-annihilation of  $\phi^0$  and  $\phi^\pm$ . This term can be written as  $\langle \sigma v_{\phi^0\phi^\pm \rightarrow \chi\chi'} \rangle \left( n_{\phi^0} n_{\phi^\pm} - n_{\phi^0}^{eq} n_{\phi^\pm}^{eq} \right)$ . Since both  $\phi^\pm$  have electromagnetic charges, they exhibit electromagnetic interaction beside weak interaction. Thus they are expected to be in thermal equilibrium with the thermal plasma by interacting electromagnetically. Therefore the number density  $n_{\phi^\pm} = n_{\phi^\pm}^{eq}$ . With this the above co-annihilation term is expressed as

$$\langle \sigma v_{\phi^0\phi^\pm \rightarrow \chi\chi'} \rangle \left( n_{\phi^0} n_{\phi^\pm} - n_{\phi^0}^{eq} n_{\phi^\pm}^{eq} \right) = [\langle \sigma v_{\phi^0\phi^\pm \rightarrow \chi\chi'} \rangle] n_{\phi^\pm}^{eq} \left( n_{\phi^0} - n_{\phi^0}^{eq} \right). \quad (40)$$

Since the number density of a non relativistic particle ( $m_{\phi^\pm} \gg T$ ) in thermal equilibrium is  $\sim T^{3/2} \exp\left(-\frac{m_{\phi^\pm}}{T}\right)$ , the contribution of the  $\phi^0\phi^\pm$  co-annihilation term (R.H.S. of Eq. 40) is exponentially suppressed. Hence this term contributes very little to the relic density of  $\phi^0$  even if  $\langle \sigma v_{\phi^0\phi^\pm \rightarrow \chi\chi'} \rangle$  is considerably large ( $\sim 10^{-8} \text{GeV}^{-2}$ ).

In the left panel of Fig. 5, we have shown the variation of  $\langle \sigma v_{\phi^0\phi^0 \rightarrow \chi\bar{\chi}} \rangle$  with parameter  $\alpha$  (Eq. (11)) for different values of  $m_{A^0}$ , namely  $m_{A^0} = 600 \text{ GeV}$ ,  $500 \text{ GeV}$ ,  $400 \text{ GeV}$ ,  $350 \text{ GeV}$ ,  $300 \text{ GeV}$ . In the right panel, the variation of  $\langle \sigma v_{SS \rightarrow \chi\bar{\chi}} \rangle$  with parameter  $\lambda_6$  (Eq. (3)) is shown. We have chosen  $m_{\phi^0} = 130 \text{ GeV}$ ,  $m_{\phi^+} = 130.2 \text{ GeV}$  and  $m_S = 130.5 \text{ GeV}$  for drawing these plots. The reason behind this choice of parameters should be cleared in the next section.

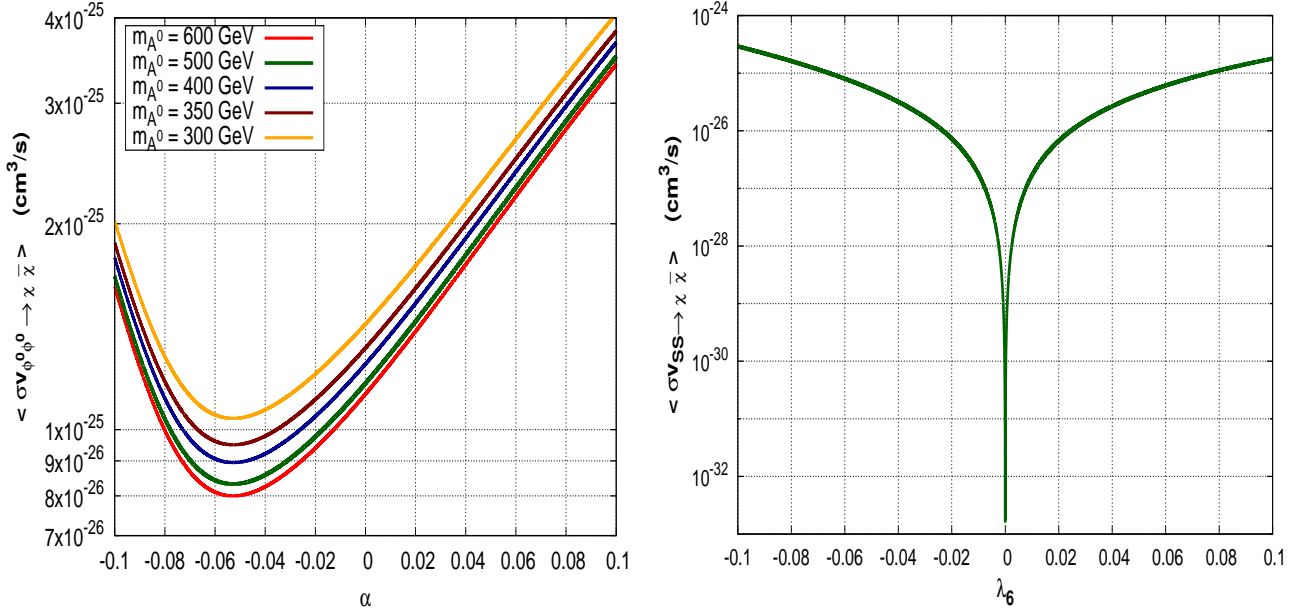


Figure 5: Left panel - Variation of  $\langle \sigma v_{\phi^0 \phi^0 \rightarrow \chi \bar{\chi}} \rangle$  with  $\alpha$  for different values of  $m_{A^0}$ , Right panel - Variation of  $\langle \sigma v_{SS \rightarrow \chi \bar{\chi}} \rangle$  with  $\lambda_6$  for  $m_S = 130.5$  GeV.

## 4 Calculation of Model Parameters

In this section we describe the procedure adopted in this work in order to estimate the values of the parameters involved in our proposed model. At the very outset, we summarise few basic requirements. In the present two component dark matter model, only the component  $\phi^0$  can account for the observed 130 GeV  $\gamma$ -line through the annihilation channel  $\phi^0 \phi^0 \rightarrow \gamma \gamma$  details of which is discussed in the next section. This is due to the fact that the other component  $S$  being a scalar singlet cannot produce sufficient annihilation cross section for the channel  $SS \rightarrow \gamma \gamma$ . So we conclude that the mass of the  $\phi^0$  component needs to be  $\sim 130$  GeV. We also find that a choice for the mass of the charged scalars,  $\phi^\pm$  (involved in the loop of the  $\phi^0 \phi^0 \rightarrow \gamma \gamma$  process, see Fig. 12) close to  $m_{\phi^0}$  enhances the annihilation cross section  $\langle \sigma v_{\phi^0 \phi^0 \rightarrow \gamma \gamma} \rangle$  (see Eq.(47)). Therefore, in order to maximise this contribution (required to achieve the cross section in the right ball park without taking a very high value for the relevant parameter in the model), we consider <sup>8</sup>  $m_{\phi^\pm} = 130.2$  GeV throughout the present discussion. Note that such a choice is consistent with the LEP bound [40]. With this consideration, the parameter  $\alpha$  is reduced to  $\sim \lambda_1/2$ .

Of course  $\phi^0$  with  $m_{\phi^0} = 130$  GeV cannot individually account for the WMAP results on

---

<sup>8</sup>The reason behind this consideration is explained in Section 5 where a complete study between the gamma-ray flux,  $\langle \sigma v_{\phi^0 \phi^0 \rightarrow \gamma \gamma} \rangle$  and  $m_{\phi^\pm}$  (see Fig. 13) is discussed in view of Eq. (41, 47, 50).

relic density. In our scenario, this deficit will be compensated by the contribution of the other component  $S$ . However we need to maximise the contribution of  $\phi^0$  to the combined relic density so as to keep the flux of the observed gamma-ray (130 GeV) from the Galactic centre at an adequate level (see Eqs.(43, 53)). For example if  $\phi^0$  contributes to 60% compared to a case where it contributes only 30% to the total relic density then the flux for the gamma-ray originated from DM ( $\phi^0$ ) annihilation will also be proportionately higher compared to the latter case. Apart from the WMAP data, we also use the limits obtained from the dark matter direct detection experiments. Needless to mention that in doing so the conditions obtained in Eqs. (12-16, 17, 18) are always satisfied.

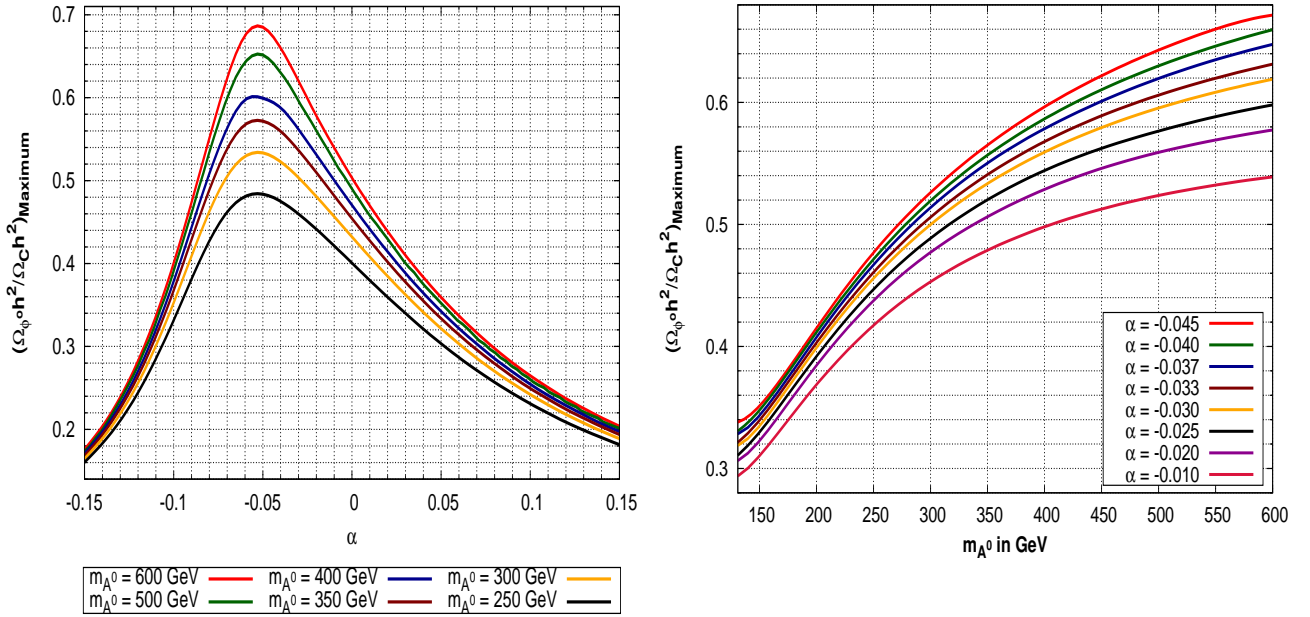


Figure 6: Left panel - Variations of  $\left(\frac{\Omega_{\phi^0} h^2}{\Omega_c h^2}\right)_{\text{Maximum}}$  with parameter  $\alpha$  for different values of  $m_{A^0}$ , Right panel - Variations of  $\left(\frac{\Omega_{\phi^0} h^2}{\Omega_c h^2}\right)_{\text{Maximum}}$  with  $m_{A^0}$  for different values of parameter  $\alpha$ .

In order to find a choice of parameter space for which the contribution from  $\phi^0$  towards relic density can be maximised, we calculate the ratio  $\left(\frac{\Omega_{\phi^0} h^2}{\Omega_c h^2}\right)$ . The relic densities  $\Omega_{\phi^0} h^2$  and  $\Omega_c h^2$  are computed using Eqs. (26, 27, 29, 30). In these computations we note that the inclusion of co-annihilation term contributes only  $\sim 0.2\%$  to the relic density of the dark matter component  $\phi^0$ . Therefore we do not consider this co-annihilation term in Boltzmann's Equation for the rest of our analysis. In the left panel of Fig. 6 we plot  $\left(\frac{\Omega_{\phi^0} h^2}{\Omega_c h^2}\right)_{\text{Maximum}}$ , as a function of the parameter  $\alpha$  for different values of  $m_{A^0}$ . Here by  $\left(\frac{\Omega_{\phi^0} h^2}{\Omega_c h^2}\right)_{\text{Maximum}}$ , we mean that we have chosen only the largest possible value of the ratio corresponding to a particular  $\alpha$  while other parameters are



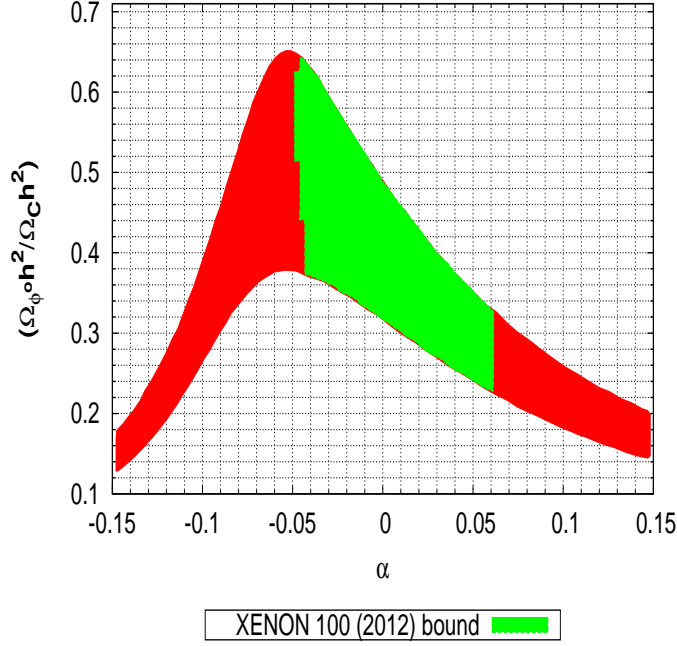


Figure 7: Variations of  $\left(\frac{\Omega_{\phi^0} h^2}{\Omega_c h^2}\right)$  with parameter  $\alpha$  for a particular value of  $m_{A^0} = 500$  GeV. The green patch corresponds to the allowed region when XENON 100 (2012) data are considered; see text for details.

scanned over their entire range ( $-0.1 \leq \lambda_6 \leq 0.1$ ,  $0.01 \leq \lambda_5 \leq 1.0$ ). From the left panel of Fig.6, our aim is to find a suitable value of  $\alpha$  for which we can have a maximum contribution to the ratio  $\left(\frac{\Omega_{\phi^0} h^2}{\Omega_c h^2}\right)$ . Note that this ratio depends on the choice of  $m_{A^0}$ . For more insight into this dependence, we show the variations of  $\left(\frac{\Omega_{\phi^0} h^2}{\Omega_c h^2}\right)_{\text{Maximum}}$  with  $m_{A^0}$  for different values of  $\alpha$  in the right panel of Fig. 6. It is evident that the contribution of  $\phi^0$  increases as  $m_{A^0}$  increases. This can also be noted from the same figure that for a fixed value of  $\alpha$ , the increase of  $\Omega_{\phi^0} h^2$  with  $m_{A^0}$  is steeper for lower values of  $m_{A^0}$ . Note that we cannot choose a value of  $m_{A^0}$  which is arbitrarily large since our choice  $m_{\phi^0} \sim m_{\phi^\pm} \sim 130$  GeV imposes a relation between parameters  $\lambda_2$  and  $\lambda_3$ , thereby one parameter can be very large. For example, to achieve  $m_{A^0} = 500$  GeV, we find  $\lambda_2 = 3.850$ ,  $\lambda_3 = -1.926$  when  $\alpha = -0.037$  is considered. The value of  $\alpha$  is so chosen that it satisfies the condition obtained from XENON 100 (2012) [35] direct detection experiment bound (Eq. (23)). The allowed region for  $\alpha$  satisfying this bound is shown in Fig. 7 (see below for discussions on Fig. 7). A choice of  $m_{A^0} = 900$  GeV would require a value of  $\lambda_2 \sim 4\pi$ , which poses a threat to the perturbativity. So for the rest of our analysis, we mostly consider  $m_{A^0} = 500$  GeV unless otherwise mentioned. With this particular choice of  $\alpha = -0.037$ , the contribution of  $\phi^0$  to the total relic density to be at most 62 %.

In Fig. 7, the same ratio (as in Fig. 6) is plotted against  $\alpha$  for a fixed value of  $m_{A^0} = 500$  GeV. Note that here the band corresponds to the variations of the parameters  $\lambda_5$  and  $\lambda_6$  respectively. In the previous Figure (left panel of Fig. 6), only maximum value of the ratio  $\left(\frac{\Omega_{\phi^0} h^2}{\Omega_c h^2}\right)$  was considered and so it was a line. Now in this Figure once we consider the XENON 100 (2012) limit on parameters  $\alpha$  and  $\lambda_6$  through Eq. (23), the initial band is restricted to only the intermediate green colour patch. We find that the ratio would be maximised to  $\sim 0.64$  for the value of  $\alpha \simeq -0.045$ , once we impose the XENON 100 (2012) data.

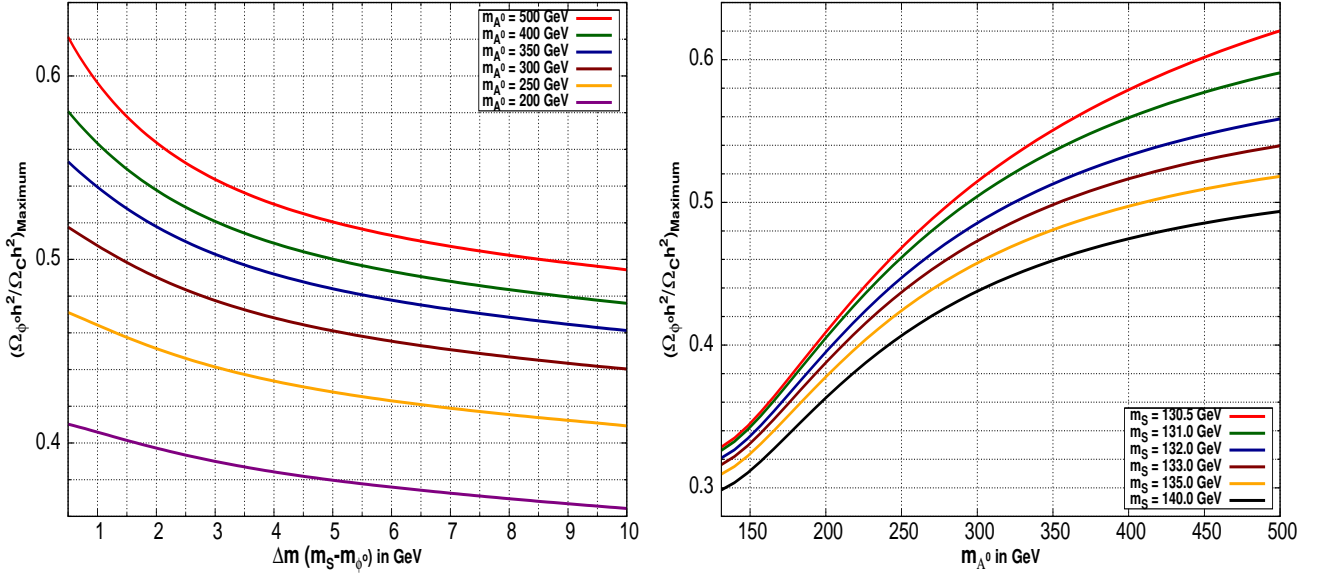


Figure 8: Left panel - Variations of  $\left(\frac{\Omega_{\phi^0} h^2}{\Omega_c h^2}\right)_{\text{Maximum}}$  with  $\Delta m(m_S - m_{\phi^0})$  for different values of  $m_{A^0}$ , Right panel - Variations of  $\left(\frac{\Omega_{\phi^0} h^2}{\Omega_c h^2}\right)_{\text{Maximum}}$  with  $m_{A^0}$  for different values of  $\Delta m(m_S - m_{\phi^0})$ .

As it is now evident that the inert doublet component alone with  $m_{\phi^0} = 130$  GeV cannot account for the total dark matter content of the universe and one needs to add the relic density of the singlet component  $S$  for producing the WMAP satisfied total relic density. In fact this is one of the motivations for choosing this two component (inert doublet + scalar singlet) dark matter model. In order to choose a suitable mass for  $S$  in the present scenario, we define a quantity  $\Delta m (= m_S - m_{\phi^0})$  remembering that  $m_S$  should be heavier than  $m_{\phi^0}$  as discussed before. We then study the variations of  $\left(\frac{\Omega_{\phi^0} h^2}{\Omega_c h^2}\right)_{\text{Maximum}}$  with  $\Delta m$  for different values of  $m_{A^0}$  which is shown in the left panel of Fig. 8. In the right panel of Fig. 8 we show the variations of the fraction  $\left(\frac{\Omega_{\phi^0} h^2}{\Omega_c h^2}\right)_{\text{Maximum}}$  with  $m_{A^0} (\leq 500 \text{ GeV})$  for different values of  $m_S$ . The plots in both the panels are obtained with  $\alpha = -0.037$  (which satisfy latest XENON 100 data). Comparing both the panels of Fig. 8 one concludes that the contribution of  $\phi^0$  to the combined relic density increases as the

mass splitting between the two components of the dark matter decreases and for this particular value of  $\alpha = -0.037$ , the ratio  $\left(\frac{\Omega_{\phi^0} h^2}{\Omega_c h^2}\right)_{\text{Maximum}}$  is  $\sim 62\%$  when  $\Delta m = 0.5$  GeV and  $m_{A^0} = 500$  GeV respectively.

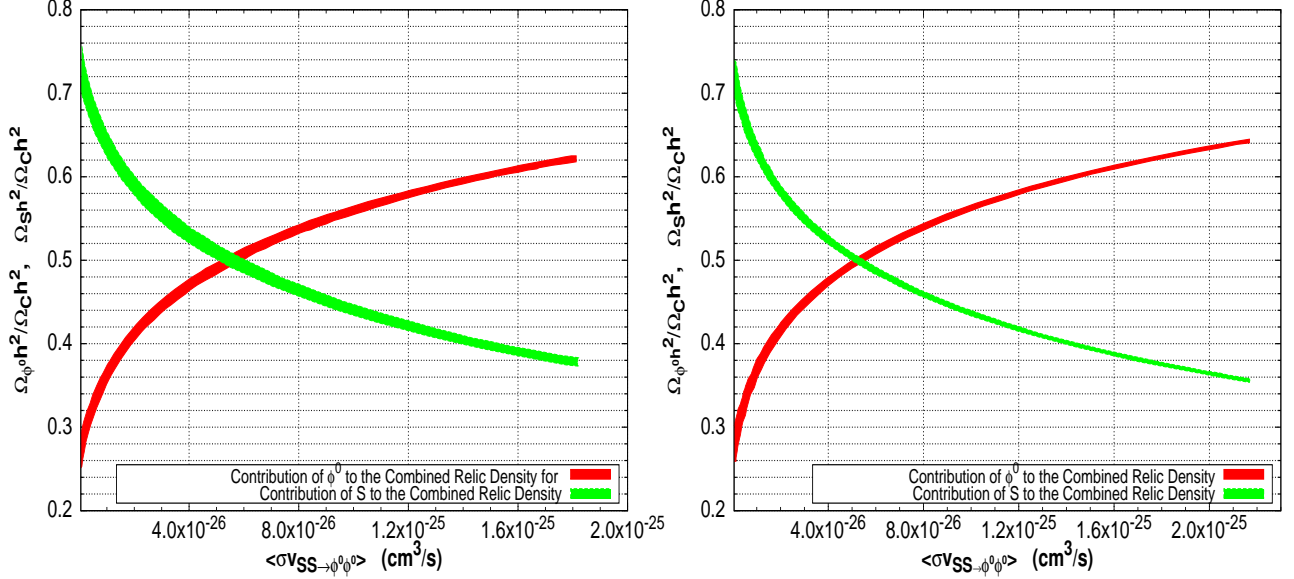


Figure 9: Variations of the contributions of  $S$  ( $\Omega_S h^2$ ) and  $\phi^0$  ( $\Omega_{\phi^0} h^2$ ) to the combined relic density ( $\Omega_c h^2$ ) with the annihilation cross section  $\langle \sigma v_{SS \rightarrow \phi^0 \phi^0} \rangle$  for two different values of  $\alpha = -0.037$  (left panel) and  $-0.045$  (right panel)

We also calculate the variations of  $\left(\frac{\Omega_{\phi^0} h^2}{\Omega_c h^2}\right)$  and  $\left(\frac{\Omega_S h^2}{\Omega_c h^2}\right)$  with the cross section  $\langle \sigma v_{SS \rightarrow \phi^0 \phi^0} \rangle$  and the results are plotted in the Fig. 9. The plots in Fig. 9 are generated with our standard set of parameter values such as  $m_{\phi^0} = 130$  GeV,  $m_{\phi^+} = 130.2$  GeV,  $m_S = 130.5$  GeV and  $m_{A^0} = 500$  GeV. The left panel of Fig. 9 is for the value of the parameter  $\alpha = -0.037$  which lies within the allowed range for  $\alpha$  as shown in Fig. 7 earlier. Similar plots in the right panel of Fig. 9 are given for comparison for the chosen value of  $\alpha = -0.045$  that corresponds to the largest allowed value of  $\left(\frac{\Omega_{\phi^0} h^2}{\Omega_c h^2}\right)$  in the present framework for XENON 100 (2012) bound (Fig. 7). From these plots, it is clear that initially when  $\langle \sigma v_{SS \rightarrow \phi^0 \phi^0} \rangle$  is very small (or nearly zero) the contribution of  $\phi^0$  is only  $\sim 25\%$  of the combined relic density. This is because for small values of  $\langle \sigma v_{SS \rightarrow \phi^0 \phi^0} \rangle$ , Eqs. (26, 27) effectively become two decoupled equations that represent the Boltzmann's equations for RSDM and IDM respectively. Under such circumstance, the calculations of the individual contributions for  $S$  and  $\phi^0$  are pursued.

Note that in this decoupled scenario, individual relic density contribution would be inversely proportional to the corresponding annihilation cross section. Therefore we need to have an estimate for  $\langle \sigma v_{\phi^0 \phi^0 \rightarrow \chi \bar{\chi}} \rangle$  and  $\langle \sigma v_{SS \rightarrow \chi \bar{\chi}} \rangle$ . In order to understand this in more detail, we refer to

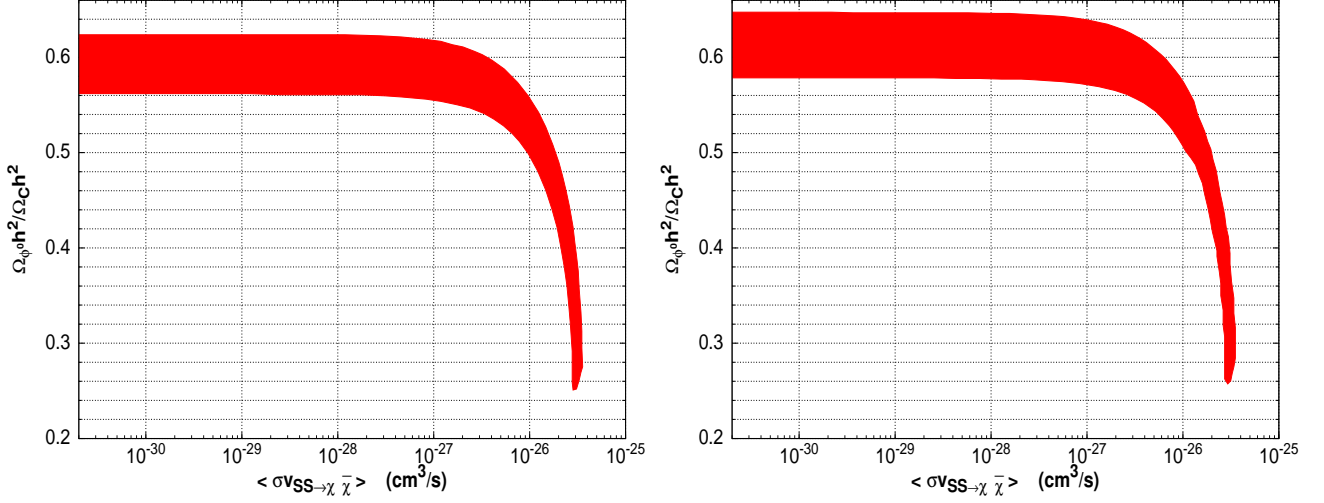


Figure 10: Variations of the contributions of  $\phi^0$  ( $\Omega_{\phi^0} h^2$ ) to the combined relic density ( $\Omega_c h^2$ ) with the annihilation cross section  $\langle \sigma v_{SS \rightarrow \chi \bar{\chi}} \rangle$  for two different values of  $\alpha = -0.037$  (left panel) and  $-0.045$  (right panel).

Fig. 5. From the left panel of Fig. 5, we see that the value of  $\langle \sigma v_{\phi^0 \phi^0 \rightarrow \chi \bar{\chi}} \rangle$  is  $\sim 8.5 \times 10^{-26} \text{ cm}^3/\text{s}$  for  $m_{A^0} = 500 \text{ GeV}$ ,  $\alpha = -0.037$ ,  $m_{\phi^0} = 130 \text{ GeV}$ ,  $m_{\phi^+} = 130.2 \text{ GeV}$ . This value of  $\langle \sigma v_{\phi^0 \phi^0 \rightarrow \chi \bar{\chi}} \rangle$  is nearly 4 times larger than what is required to get WMAP satisfied relic density for dark matter mass of 130 GeV, thereby contributing only  $\sim 25\%$  to the total relic density (Eq. (19)) as seen from left panel of Fig. 9. So we would expect that the rest  $\sim 75\%$  contribution should come from the singlet scalar component  $S$  in the present model. This is indeed possible if we consider the right panel of Fig. 5. This corresponds to a case where practically there is no interactions between  $S$  and  $\phi^0$ , i.e.  $\lambda_5 \simeq 0$ . As the interaction between  $S$  and  $\phi^0$  becomes increasingly stronger (i.e.  $|\lambda_5|$  starts to have nonzero value), more and more  $S$  particles annihilate to produce  $\phi^0$  particles and contribution of  $\phi^0$  to the combined relic density will be boosted. It reaches a maximum which comes out to be  $\sim 62\%$  ( $\sim 64\%$ ) in our present analysis for  $\alpha = -0.037$  ( $\alpha = -0.045$ ) for  $\langle \sigma v_{SS \rightarrow \phi^0 \phi^0} \rangle \sim 1.8 \times 10^{-25} \text{ cm}^3/\text{s}$  ( $\sim 2.2 \times 10^{-25} \text{ cm}^3/\text{s}$ ) seen from the left panel (right panel) of Fig. 9.

Fig. 10 shows the variation of  $\left( \frac{\Omega_{\phi^0} h^2}{\Omega_c h^2} \right)$  with  $\langle \sigma v_{SS \rightarrow \chi \bar{\chi}} \rangle$ . Similar set of parameters as in Fig. 9 are adopted in generating the two plots of Fig. 10. Likewise in Fig. 9 the right panel of Fig. 10 corresponds to  $\alpha = -0.045$  and is given for comparison with the left panel ( $\alpha = -0.037$ , adopted value in this calculation) of this figure. The plots indicate that the contribution of  $\phi^0$  to the combined relic density decreases as the value of  $\langle \sigma v_{SS \rightarrow \chi \bar{\chi}} \rangle$  increases. This is because of the increment of  $\langle \sigma v_{SS \rightarrow \chi \bar{\chi}} \rangle$  signifies large number  $S$  particles annihilate into SM particles and consequently less number of particles are available for annihilation of  $S$  to produce  $\phi^0$  in the final

state. As a result the relic density of  $\phi^0$  decreases. From the left panel of Fig. 10, we conclude that in order to obtain the relic density contribution of  $\phi^0$  close to 62% or above the value of  $\langle\sigma v_{SS\rightarrow\chi\bar{\chi}}\rangle$  should be  $\lesssim 1.74 \times 10^{-28} \text{cm}^3/\text{s}$ . Note that the parameter  $\lambda_6$  is involved both in  $\langle\sigma v_{SS\rightarrow\chi\bar{\chi}}\rangle$  and  $\langle\sigma v_{SS\rightarrow\phi^0\phi^0}\rangle$ , whereas the parameter  $\lambda_5$  appeared only in  $\langle\sigma v_{SS\rightarrow\phi^0\phi^0}\rangle$ . Therefore this limit (on  $\langle\sigma v_{SS\rightarrow\chi\bar{\chi}}\rangle$ ) along with the other one we just discussed above,  $\langle\sigma v_{SS\rightarrow\phi^0\phi^0}\rangle \sim 1.8 \times 10^{-25} \text{cm}^3/\text{s}$ , set up a range of allowed region of  $\lambda_5$  and  $\lambda_6$  if we restrict ourselves with  $\left(\frac{\Omega_{\phi^0} h^2}{\Omega_c h^2}\right) \sim 62\%$ . The allowed range of values of the parameters  $\lambda_5$ ,  $\lambda_6$  for the present case ( $m_{A^0} = 500 \text{ GeV}$ ) is shown in the left panel of Fig. 11. In Table 2 we furnish the values of the parameters  $\lambda_5$  and  $\lambda_6$  along with other model parameters.

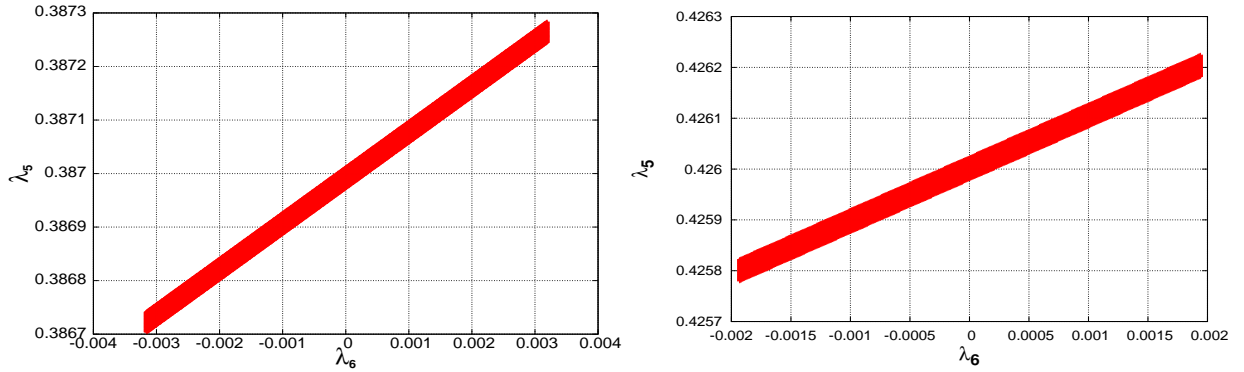


Figure 11: Left panel - Allowed range of the parameters  $\lambda_5, \lambda_6$  for the parameter  $\alpha = -0.037$ . Right panel - Allowed range of the parameters  $\lambda_5, \lambda_6$  for the parameter  $\alpha = -0.045$ . Both plots are drawn for  $m_{\phi^0} = 130 \text{ GeV}$ ,  $m_{\phi^+} = 130.2 \text{ GeV}$ ,  $\Delta m = 0.5 \text{ GeV}$ ,  $m_{A^0} = 500 \text{ GeV}$ .

Similarly, from the right panel of Fig. 10 we conclude that in order to obtain  $\left(\frac{\Omega_{\phi^0} h^2}{\Omega_c h^2}\right) \sim 64\%$ , one should have  $\langle\sigma v_{SS\rightarrow\chi\bar{\chi}}\rangle \lesssim 0.65 \times 10^{-28} \text{cm}^3/\text{s}$ . The corresponding allowed region in  $\lambda_5$ - $\lambda_6$  parameter space is shown in the right panel of Fig. 11. The values of other parameters for this present scenario ( $\alpha = -0.045$ ) which produces the largest possible contribution of  $\phi^0$  towards the total relic density are also tabulated in Table 3.

## 5 130 GeV $\gamma$ -ray line from Dark Matter annihilation

In this section our endeavour will be to explain the recently observed 130 GeV  $\gamma$ -line from the Galactic centre originated from dark matter annihilation in the framework of the present two component dark matter model. In order to produce such a 130 GeV  $\gamma$ -line, the required DM annihilation cross section into two photons should be  $\sim 10^{-27} \text{cm}^3/\text{s}$  as predicted from the analysis [1, 3] of Fermi-LAT data [2]. In the context of the present two component dark matter

Mass of $A^0$ ( $m_A^0$ ) (GeV)	Contribution of $\phi^0$ in the combined Relic Density	$\mu_2$ (GeV)	$\lambda_1$	$\lambda_5$	$ \lambda_6 $	$\lambda_2$	$\lambda_3$
300	51.7%	138.344	-0.072	0.2698 - 0.2703	$\leq 2.6 \times 10^{-3}$	1.206	-0.604
350	55.3%	138.344	-0.072	0.3014 - 0.3020	$\leq 2.8 \times 10^{-3}$	1.743	-0.872
400	58.1%	138.344	-0.072	0.3322 - 0.3327	$\leq 2.8 \times 10^{-3}$	2.363	-1.182
500	62.1%	138.344	-0.072	0.3867 - 0.3873	$\leq 3.2 \times 10^{-3}$	3.850	-1.926

Table 2: Relic density contribution of  $\phi^0$  for different values of  $m_A^0$  with the corresponding values of other model parameters are  $\alpha = -0.037$ ,  $\Delta m = 0.5$  GeV ( $m_S = 130.5$  GeV,  $m_{\phi^0} = 130.0$  GeV).

Mass of $A^0$ ( $m_A^0$ ) (GeV)	Contribution of $\phi^0$ in the combined Relic Density	$\mu_2$ (GeV)	$\lambda_1$	$\lambda_5$	$ \lambda_6 $	$\lambda_2$	$\lambda_3$
500	64.4%	140.083	-0.088	0.4258 - 0.4262	$\leq 1.9 \times 10^{-3}$	3.850	-1.926

Table 3: Maximum Relic density contribution of  $\phi^0$  for  $m_A^0 = 500$  GeV,  $\alpha = -0.045$ ,  $\Delta m = 0.5$  GeV ( $m_S = 130.5$  GeV,  $m_{\phi^0} = 130.0$  GeV).

model, only the  $\phi^0$  component having mass 130 GeV can contribute to the production of 130 GeV  $\gamma$ -ray line. The annihilation of  $\phi^0\phi^0$  into  $\gamma\gamma$  can take place only via charged scalar  $\phi^\pm$  and  $W^\pm$  loops. It can indeed produce the required cross section  $\sim 10^{-27}$  cm<sup>3</sup>/s. The cross sections for other annihilation channels that can produce  $\gamma\gamma$  (e.g. via Higgs) for both the components  $\phi^0$  and  $S$  are orders of magnitude less than this value [21].

We calculate the  $\gamma$ -ray flux due to annihilation of  $\phi^0$  in the “central region” of our Milky way galaxy. The lowest order Feynman diagrams for the process  $\phi^0\phi^0 \rightarrow \gamma\gamma$  via  $\phi^\pm$  and  $W^\pm$  loops are shown in Fig. 12. The expression of differential  $\gamma$ -ray flux due to dark matter annihilation in galactic halo is given by [41],

$$\frac{d\Phi_\gamma}{dE_\gamma} = \frac{1}{8\pi} \frac{\langle \sigma v_{\phi^0\phi^0 \rightarrow \gamma\gamma} \rangle}{m_{\phi^0}^2} \frac{dN_\gamma}{dE_\gamma} r_\odot \rho_\odot^2 \bar{J}, \quad (41)$$

where  $r_\odot = 8.5$  kpc is the distance of the sun from the Galactic centre and  $\rho_\odot = 0.4$  GeV/cm<sup>3</sup> is the the local dark matter density at the solar neighbourhood. The quantity  $\bar{J}$  in the above is

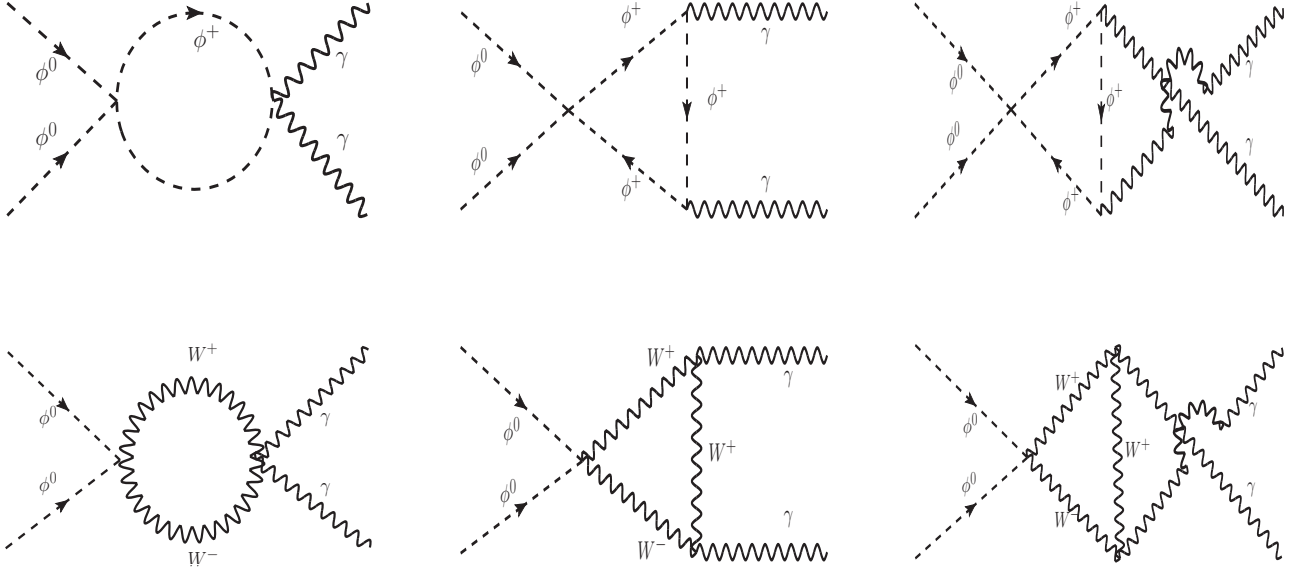


Figure 12: Lowest order Feynman diagrams for the process  $\phi^0 \phi^0 \rightarrow \gamma \gamma$

given by

$$\bar{J} = \frac{4}{\Delta\Omega} \int dl \int db \cos b J(l, b) , \quad (42)$$

with

$$J(l, b) = \int_{l.o.s} \frac{ds}{r_\odot} \left( \frac{\rho(r)}{\rho_\odot} \right)^2 , \quad (43)$$

and

$$\Delta\Omega = 4 \int dl \int db \cos b . \quad (44)$$

Here  $l$  and  $b$  in Eqs. (42, 44) are galactic longitude and latitude respectively. In the above, the integration is performed around a radius of  $3^\circ$  (galactic central region) around a centre with coordinates  $(l, b) = (-1^\circ, -0.7^\circ)$  [3]. In Eq. (43)  $r$  and  $s$  are related by,

$$r = (s^2 + r_\odot^2 - 2sr_\odot \cos l \cos b)^{1/2} . \quad (45)$$

The expression of the energy spectrum of  $\gamma$ , denoted by  $\frac{dN_\gamma}{dE_\gamma}$  is given by,

$$\frac{dN_\gamma}{dE_\gamma} = 2\delta(E - E_\gamma) . \quad (46)$$

We have performed  $l, b$  integration (in Eqs. (42, 44)) over the “central region” of our galaxy and the  $s$  integration (in Eq. 43) is along the line of sight (l.o.s).

We explicitly calculate all the Feynman diagrams given in Fig. 12 and obtain the expression for  $\langle \sigma v_{\phi^0 \phi^0 \rightarrow \gamma \gamma} \rangle$  as

$$\langle \sigma v_{\phi^0 \phi^0 \rightarrow \gamma \gamma} \rangle = \frac{\alpha^2 m_{\phi^0}^2}{32\pi^3} \left| \frac{g_{\phi^0 \phi^0 \phi^+ \phi^-} F_{\phi^+}}{m_{\phi^+}^2} - \frac{g_{\phi^0 \phi^0 W^+ W^-} F_W}{m_W^2} \right|^2. \quad (47)$$

Where

$$\begin{aligned} F_{\phi^+} &= \tau[1 - \tau f(\tau)] , \\ F_W &= 2 + 3\tau + 3\tau(2 - \tau)f(\tau) , \end{aligned} \quad (48)$$

with  $\tau = \frac{m_i^2}{m_{\phi^0}^2}$ ,  $i = \phi^\pm, W^\pm$  and

$$f(\tau) = \begin{cases} \left[ \sin^{-1}(\sqrt{1/\tau}) \right]^2 , & \text{for } \tau \geq 1 , \\ -\frac{1}{4} \left[ \ln \frac{1 + \sqrt{1-\tau}}{1 - \sqrt{1-\tau}} - i\pi \right]^2 , & \text{for } \tau < 1 . \end{cases} \quad (49)$$

Since the couplings  $g_{\phi^0 \phi^0 \phi^+ \phi^-} = -\rho_2$  and  $g_{\phi^0 \phi^0 W^+ W^-} = \frac{m_W^2}{v^2}$  (see Table 1), Eq. (47) can be written as

$$\langle \sigma v_{\phi^0 \phi^0 \rightarrow \gamma \gamma} \rangle = \frac{\alpha^2 m_{\phi^0}^2}{32\pi^3} \left| \frac{\rho_2 F_{\phi^+}}{m_{\phi^+}^2} + \frac{F_W}{v^2} \right|^2. \quad (50)$$

In the present work,  $\gamma$ -ray flux is calculated for two different dark matter halo profiles namely the NFW profile [29] and the Einasto profile [30]. These halo profiles give the functional dependence of dark matter density  $\rho(r)$  with  $r$ . The expression of  $\rho(r)$  for the NFW profile is given by,

$$\rho_{\text{NFW}}(r) = \frac{\rho_s}{(r/r_s)(1 + r/r_s)^2}, \quad (51)$$

and for the Einasto profile

$$\rho_{\text{Einasto}}(r) = \rho_s \exp \left\{ -\frac{2}{\gamma} \left[ \left( \frac{r}{r_s} \right)^\gamma - 1 \right] \right\}, \quad (52)$$

where  $r_s$  in Eqs. (51-52) is taken to be 20 kpc and  $\gamma = 0.17$  in Eq. (52). In the above the value of the normalisation constant  $\rho_s$  is determined by demanding that at  $r = r_\odot$ , the density  $\rho(r) = \rho_\odot$ . We have seen earlier that in the present model of two component dark matter, the



Mass of $A^0$ (GeV)	$\left(\frac{\Omega_{\phi^0} h^2}{\Omega_c h^2}\right)$	$\rho'_\odot$ (GeV/cm <sup>3</sup> )	$\rho_s$ (GeV/cm <sup>3</sup> )	$\langle\sigma v_{\phi^0\phi^0\rightarrow\gamma\gamma}\rangle$ (cm <sup>3</sup> /s)	$\rho_2$
500	0.621	0.248	0.214	$1.187^{+0.405}_{-0.344} \times 10^{-27}$	$5.34^{+0.72}_{-0.72}$
400	0.581	0.232	0.201	$1.347^{+0.460}_{-0.392} \times 10^{-27}$	$5.64^{+0.76}_{-0.77}$
350	0.553	0.221	0.191	$1.490^{+0.505}_{-0.434} \times 10^{-27}$	$5.89^{+0.79}_{-0.81}$
300	0.517	0.207	0.178	$1.717^{+0.586}_{-0.500} \times 10^{-27}$	$6.26^{+0.85}_{-0.86}$

Table 4: Results for the NFW Profile for  $\alpha = -0.037$ .

inert doublet component  $\phi^0$  contributes to  $\sim 62\%$   $\left(\frac{\Omega_{\phi^0} h^2}{\Omega_c h^2} \sim 0.62\right)$  of the total dark matter relic density. Therefore in calculating the  $\gamma$ -ray flux from the process  $\phi^0\phi^0 \rightarrow \gamma\gamma$  we compute  $\rho_s$  by taking

$$\rho'_\odot = \rho_\odot \times \frac{\Omega_{\phi^0} h^2}{\Omega_c h^2}, \quad (53)$$

and demanding that for the dark matter component  $\phi^0$ ,  $\rho(r) = \rho'_\odot$  at  $r = r_\odot$  with  $\rho_\odot = 0.4$  GeV/cm<sup>3</sup> [42].

From the left panel of Fig. 3 of Ref. [3] the best fit value of the  $\gamma$ -ray flux (in terms of  $E^2\Phi$  (GeV cm<sup>-2</sup> s<sup>-1</sup> sr<sup>-1</sup>)) observed by Fermi-LAT from the central signal region of the Galaxy can be read as  $E^2\Phi = 5.6 \times 10^{-5}$  GeV cm<sup>-2</sup> s<sup>-1</sup> sr<sup>-1</sup> with 95% C.L. error band that lies in the range  $3.97 \times 10^{-5} \leq E^2\Phi \leq 7.51 \times 10^{-5}$  (GeV cm<sup>-2</sup> s<sup>-1</sup> sr<sup>-1</sup>). We use these values of the flux in Eq. (41) and compute  $\langle\sigma v_{\phi^0\phi^0\rightarrow\gamma\gamma}\rangle$  for the best fit value of the flux as also the two extremities of its error band at 130 GeV. Note that the parameter  $\rho_2$  is yet to be determined. This can be estimated by calculating the cross section  $\langle\sigma v_{\phi^0\phi^0\rightarrow\gamma\gamma}\rangle$  (given by Eq. (50)) and hence the flux ( $E^2\Phi$ ) and then comparing this flux with that given by the Fermi-LAT data.

The results are furnished in Table 4 and Table 5 for the NFW profile and the Einasto profile respectively. They are given for the chosen mass  $m_{A^0}$  of 500 GeV as also for three other values of

Mass of $A^0$ (GeV)	$\left(\frac{\Omega_{\phi^0} h^2}{\Omega_c h^2}\right)$	$\rho'_\odot$ (GeV/cm <sup>3</sup> )	$\rho_s$ (GeV/cm <sup>3</sup> )	$\langle\sigma v_{\phi^0\phi^0\rightarrow\gamma\gamma}\rangle$ (cm <sup>3</sup> /s)	$\rho_2$
500	0.621	0.248	0.051	$0.606^{+0.207}_{-0.176} \times 10^{-27}$	$4.01^{+0.54}_{-0.55}$
400	0.581	0.232	0.047	$0.714^{+0.243}_{-0.208} \times 10^{-27}$	$4.30^{+0.58}_{-0.58}$
350	0.553	0.221	0.045	$0.789^{+0.255}_{-0.227} \times 10^{-27}$	$4.47^{+0.59}_{-0.61}$
300	0.517	0.207	0.042	$0.894^{+0.305}_{-0.260} \times 10^{-27}$	$4.74^{+0.63}_{-0.65}$

Table 5: Results for the Einasto Profile for  $\alpha = -0.037$ .

$m_{A^0}$  namely 400, 350, 300 GeV for the purpose of demonstration where  $\alpha = -0.037$ . In both the Tables 4, 5 the values of the cross sections obtained for the best fit value of the flux are given. The computed cross sections for the two extremities of the error band of the flux are shown by the subscripts and superscripts of the central values. The corresponding values of  $\rho_2$  that are calculated using Eq. (50) are also shown in similar fashion. It is seen from both the Tables that although the calculated values for  $\rho_2$  depend on the dark matter density profile that one chooses, they are within the perturbative limit and the corresponding cross sections  $\langle\sigma v_{\phi^0\phi^0\rightarrow\gamma\gamma}\rangle$  are also within the desired limits of  $\sim 10^{-27}$  cm<sup>3</sup>/s. In Table 6 we show the similar set of values (like Tables 4 and 5) for another value of  $\alpha = -0.045$ .

Here we like to mention that we have checked the possibility that the continuum gamma-rays may overshoot the monochromatic gamma-ray line. In Ref. [17], the authors have shown that in order to distinguish the monochromatic gamma-line (from DM DM  $\rightarrow \gamma\gamma$  channel) from the continuum gamma-ray spectrum (produced by the secondary photons originating from the annihilation products of dark matter e.g. gauge bosons,  $q\bar{q}$ ,  $f\bar{f}$ ), the branching ratio for the channel DM DM  $\rightarrow \gamma\gamma$  must be greater than 1% of total annihilation cross section (sum of annihilation cross sections for all possible channels). For the dark matter component  $\phi^0$  in our

Name of the halo profile	Mass of $A^0$ (GeV)	$\left(\frac{\Omega_{\phi^0} h^2}{\Omega_c h^2}\right)$	$\rho'_\odot$ (GeV/cm <sup>3</sup> )	$\rho_s$ (GeV/cm <sup>3</sup> )	$\langle\sigma v_{\phi^0\phi^0\rightarrow\gamma\gamma}\rangle$ (cm <sup>3</sup> /s)	$\rho_2$
NFW	500	0.644	0.258	0.222	$1.104^{+0.375}_{-0.324} \times 10^{-27}$	$5.18^{+0.69}_{-0.71}$
Einasto	500	0.644	0.258	0.052	$0.584^{+0.196}_{-0.171} \times 10^{-27}$	$3.95^{+0.52}_{-0.55}$

Table 6: Results for NFW and Einasto profile for the value of  $\alpha = -0.045$ ,  $m_{A^0} = 500$  GeV,  $m_{\phi^+} = 130.2$  GeV.

model we find that this ratio is nearly  $1/70$  (i.e.  $> 10^{-2}$ ) as seen from the left panel of Fig. 5 and Table 4.

A discussion on the choice of the value of charged scalar mass  $m_{\phi^+}$  is in order. In this work the value  $m_{\phi^+} = 130.2$  GeV is adopted. The viability of such a choice is demonstrated in Fig. 13. In the left panel of Fig. 13 we show the variations of  $\langle\sigma v_{\phi^0\phi^0\rightarrow\gamma\gamma}\rangle$  for different values of  $m_{\phi^+}$ . We have excluded the situation  $m_{\phi^+} < m_{\phi^0}$  ( $m_{\phi^0}$  is fixed at 130 GeV), which can give rise to the possibility of having charged relic in the present scenario (with an unbroken  $Z_2$ ). The abundance of such a charged relic is severely constrained [44] which therefore prompts us to analyse the  $\langle\sigma v_{\phi^0\phi^0\rightarrow\gamma\gamma}\rangle$  for those values of  $m_{\phi^+}$  which satisfy  $m_{\phi^+} > m_{\phi^0}$ . We have checked with  $m_{\phi^+} \sim 130.2$  GeV,  $\phi^+$  can actually decay<sup>9</sup> (e.g.  $\phi^+ \rightarrow \phi^0 + e^+ + \nu_e$ ) [45] before Big Bang Nucleosynthesis (BBN). We find that the annihilation cross section  $\langle\sigma v_{\phi^0\phi^0\rightarrow\gamma\gamma}\rangle$  of  $\phi^0$  to produce  $\gamma$  decreases sharply with the increase of  $m_{\phi^+}$  as is evident from the left panel of Fig. 13. The variations of the gamma-ray flux with  $m_{\phi^+}$  are also displayed in the right panel of Fig. 13. Calculations for both the plots in Fig. 13 are carried out for a chosen value of  $\rho_2$  (see Table 6) such that the best fit value of the gamma-ray flux from the Fermi-LAT data can be reproduced with  $m_{\phi^+} = 130.2$  GeV. Also in the right panel, we include the flux (the best fit value) of energy 130 GeV obtained from Fermi-LAT data along with its error band of 95% C.L. We therefore conclude that  $m_{\phi^+}$  which would produce gamma-ray flux within 95% C.L. of the experimental observation should lie in a very narrow interval (with a particular choice of other parameters involved), in the vicinity of  $m_{\phi^0}$  but not below it. For demonstrative purpose, we have shown

---

<sup>9</sup>decay width turns out to be of the order of  $\simeq 10^{-16}$  GeV.

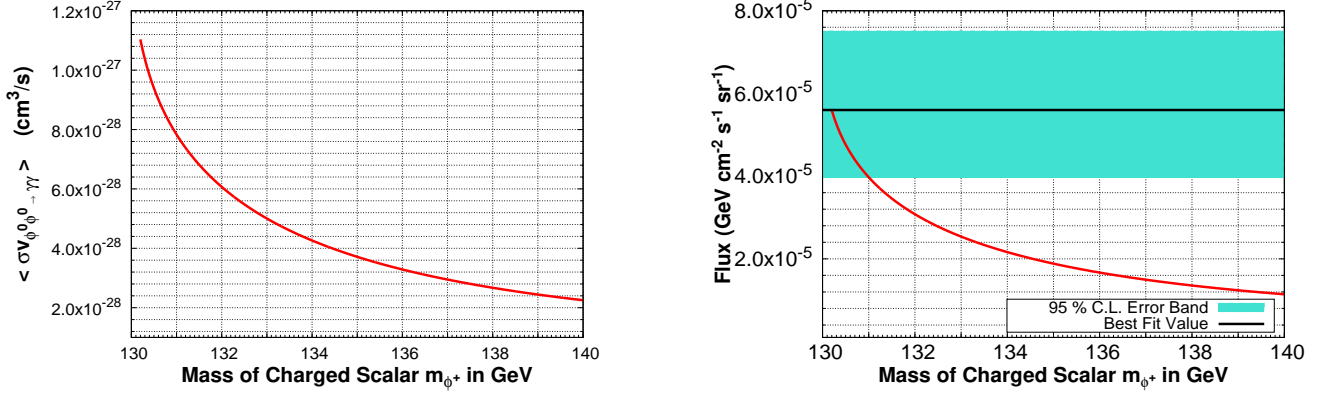


Figure 13: Left panel - Variations of  $\langle \sigma v_{\phi^0\phi^0 \rightarrow \gamma\gamma} \rangle$  with the mass of charged scalar ( $m_{\phi^+}$ ). Right panel - Variations of gamma-ray flux with  $m_{\phi^+}$ , with 95% C.L. error band and the best fit value of the gamma-ray flux from Fermi-LAT data are represented by turquoise colour band and black solid line respectively.

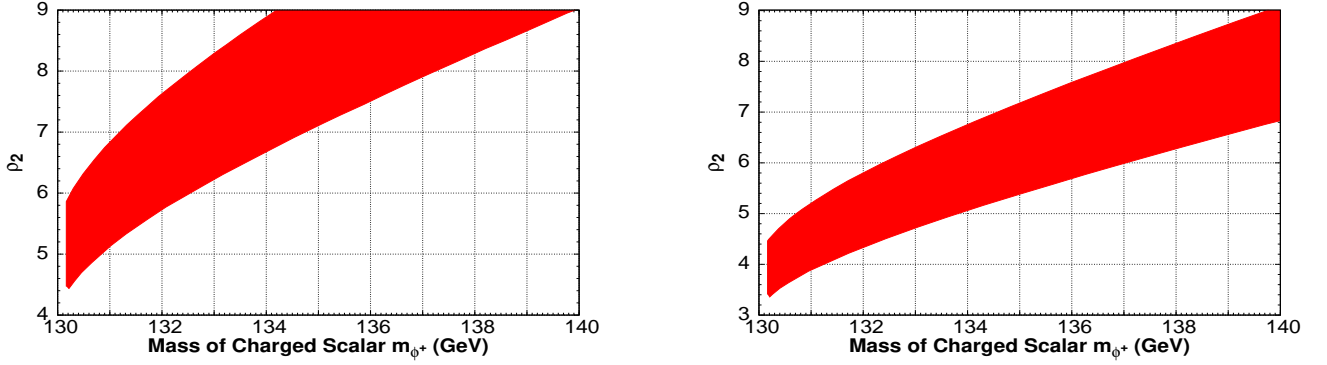


Figure 14: Variations of  $\rho_2$  with charged scalar mass  $m_{\phi^+}$  for both NFW (left panel) and Einasto (right panel) profile.

two contour plots of the parameter  $\rho_2$  vs  $m_{\phi^+}$  in both the panels of Fig. 14. These contours are drawn for both NFW and Einasto profile respectively where each point within the contours produces gamma-ray flux which lies within the 95% C.L. of observed flux from Fermi-LAT data. It is seen from both the panels of Fig. 14 that a higher value of  $m_{\phi^+}$  is also possible but at the expense of a high value of the coupling  $\rho_2$ . However, we restrict ourselves with the choice  $m_{\phi^+} = 130.2$  GeV for the rest of our discussion.

## 6 Discussions and Conclusions

In the present work we propose a dark matter model which contains two dark matter candidates. Such a two component dark matter model can be obtained by adding a scalar singlet  $S$  (singlet under SM gauge group) and a doublet  $\Phi$  (doublet under SM gauge group) to the scalar sector of SM. We have introduced discrete symmetry  $Z_2 \times Z'_2$  under which only  $S$  and  $\Phi$  transform non-trivially. Both the scalar singlet  $S$  and doublet  $\Phi$  do not produce any VEV. Consequently  $Z_2 \times Z'_2$  symmetry remains unbroken which ensure the stability of both the components ( $S, \phi^0$ ) of the dark matter in the present model. While the component  $\phi^0$  (neutral part of the doublet  $\Phi$ ) can produce the annihilation cross section required to obtain 130 GeV  $\gamma$ -line, the value of the corresponding cross section for the scalar singlet component  $S$  falls deficit by few orders of magnitude. However the component  $\phi^0$  above, having a mass of 130 GeV cannot solely account for the relic density predicted by WMAP. This deficit in relic density is compensated by the scalar singlet component  $S$  such that the combined relic density ( $\Omega_c h^2$ ) for this two component dark matter model always lies within the range given by WMAP. Combined relic density is the sum of individual relic densities of both the components  $S$  and  $\phi^0$  which are obtained by solving the coupled Boltzmann's equations numerically. We have found that the contribution of the component  $\phi^0$  to  $\Omega_c h^2$  will be  $\sim 62\%$  ( $\sim 64\%$ ) when we consider  $\alpha = -0.037$  ( $-0.045$ ),  $|\lambda_6| \leq 3.2 \times 10^{-3}$  ( $\leq 1.9 \times 10^{-3}$ )<sup>10</sup>,  $\Delta m = 0.5$  GeV,  $\lambda_5 \sim 0.387$  ( $\sim 0.426$ ) and  $m_{A^0} = 500$  GeV. Finally in the last section we have calculated the annihilation cross section  $\langle \sigma v_{\phi^0 \phi^0 \rightarrow \gamma\gamma} \rangle$  for the channel  $\phi^0 \phi^0 \rightarrow \gamma\gamma$  with the mass of  $\phi^0 \sim 130$  GeV. Using the expression of this annihilation cross section ( $\langle \sigma v_{\phi^0 \phi^0 \rightarrow \gamma\gamma} \rangle$ ) we have computed the  $\gamma$ -ray flux of energy 130 GeV for two different dark matter halo profiles namely the NFW profile and the Einasto profile. The exact dark matter density at the galactic centre is unknown (e.g. Ref. [41] and references therein). This may produce an additional uncertainty in the flux calculation. Depending on the value of the dark matter density at the galactic centre, 130 GeV gamma-line may also be produced for a value of annihilation cross section lower than the specified value of  $\sim 10^{-27}$  cm<sup>3</sup>/s. Fermi Collaboration placed an upper limit [43]  $\langle \sigma v_{\gamma\gamma} \rangle < 1.4 \times 10^{-27}$  cm<sup>3</sup>/s for 130 GeV dark matter with an NFW profile and  $\langle \sigma v_{\gamma\gamma} \rangle < 1.0 \times 10^{-27}$  cm<sup>3</sup>/s with an Einasto profile. In the present work we indeed obtain  $\sigma v_{\gamma\gamma}$  in the range of this upper limit ( $\sim 10^{-27}$  cm<sup>3</sup>/s).

As a typical set of parameter space of the model under consideration, we have tabulated values of all the parameters for specific choice of  $\alpha = -0.045$  ( $\alpha = -0.037$ ) in Table 3 (Table 2), which can contribute towards the DM relic density at an appropriate level as well as produce the 130 GeV gamma-ray. It can be noticed that among all these parameters, the quartic couplings

---

<sup>10</sup>both  $\alpha$  and  $\lambda_6$  satisfy XENON 100 (2012) [35] limit as well as limits from other dark matter direct detection experiments namely CDMS-II [46], EDELWEISS-II [47] etc.

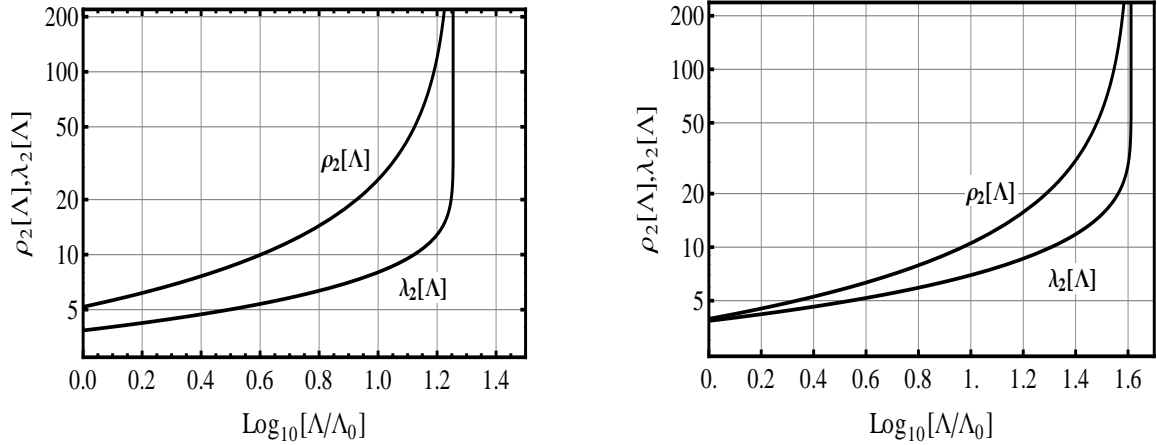


Figure 15: Variation of the couplings  $\rho_2$  and  $\lambda_2$  with energy scale  $\Lambda$  for both NFW (left panel) and Einasto (right panel) profile.

$\rho_2$  (between  $\phi^0$  and  $\phi^\pm$ , responsible for the production of 130 GeV  $\gamma$  line, see Fig. 12) and  $\lambda_2$  (related to the mass of  $A^0$ ) are rather on the higher side. A comment on this particular choice of  $m_{A^0}$  is relevant here. A heavier  $A^0$  indicates a larger choice of  $\lambda_2$  as seen from Table 2. Although a larger  $m_{A^0}$  would maximise the contribution of  $\phi^0$  towards DM relic density (i.e. to get a larger ratio  $\left(\frac{\Omega_{\phi^0} h^2}{\Omega_c h^2}\right)$ , see Fig. 6), we keep  $m_{A^0}$  at 500 GeV so that the corresponding parameter  $\lambda_2$  can have a not-very-large value. As the couplings (particularly  $\rho_2$  and  $\lambda_2$ ) becomes stronger at high energy scale, it would pose a threat to the validity of the model as the theory tends to be non-perturbative at some high energy scale. In this scenario we have estimated the Landau pole ( $\Lambda_L$ ) of the model. We have used the one loop beta functions [27, 48] appropriate for our inert Higgs doublet and singlet model. Using the parameters in Table 3 as an initial choice at a energy scale  $\Lambda_0 = m_{\phi^0} = 130$  GeV, we plot the running of  $\rho_2$  and  $\lambda_2$  in both panels of Fig. 15. We find that for  $\alpha = -0.045$ ,  $\Lambda_L \sim 2.5$  TeV ( $\sim 5$  TeV) when NFW (Einasto) dark matter profile is considered. Similar results are obtained for the case with  $\alpha = -0.037$  (note that the mass  $m_{A^0}$  of the only massive field  $A^0$  is well within these limits).

Since the present two component dark matter consists of a singlet scalar and an SU(2) inert doublet, they have different couplings with Higgs boson (Eqs. (3, 4)). The doublet component will also have additional interactions with gauge bosons. Hence both the scattering cross section and the annihilation cross section for each of the two components are different even though they have masses close to each other in the present model. Therefore the rate of direct detection and its subsequent variations with the recoil energies for the two components will be different. Also in the event that the scalar and inert doublet components of this two component dark matter are captured by the gravity of the solar core and each component suffers subsequent annihilations in

the core yielding neutrinos as the final states then the spectra and the fluxes for such neutrinos will differ depending on which component of the dark matter (scalar singlet or inert doublet) annihilates to produce them. Similar features would also be realised if these two dark matter components annihilate to produce gamma-rays at a suitable dense site such as galactic centre. If the measurements of such “GeV neutrinos” from the solar core exhibit two distinct natures for both the flux and spectrum and if such a difference can be corroborated with the possible gamma-ray signal from the galactic centre then this may indicate a probable indirect detection of such a two component dark matter.

**Acknowledgments** : A.B. would like to thank P. B. Pal, A. Ghosal and D. Adak for useful suggestions and discussions. The authors thank J. Kopp, M. Raidal and K. Kannike for very useful suggestions and comments. A.S acknowledges the support from the Start Up grant from IIT Guwahati.

## References

- [1] T. Bringmann, X. Huang, A. Ibarra, S. Vogl and C. Weniger, JCAP **1207**, 054 (2012) [arXiv:1203.1312 [hep-ph]], C. Weniger, JCAP **1208**, 007 (2012) [arXiv:1204.2797 [hep-ph]].
- [2] W. B. Atwood *et al.* [LAT Collaboration], Astrophys. J. **697**, 1071 (2009) [arXiv:0902.1089 [astro-ph.IM]].
- [3] E. Tempel, A. Hektor and M. Raidal, JCAP **1209**, 032 (2012) [Addendum-ibid. **1211**, A01 (2012)] [arXiv:1205.1045 [hep-ph]].
- [4] M. Su and D. P. Finkbeiner, arXiv:1206.1616 [astro-ph.HE].
- [5] A. Hektor, M. Raidal and E. Tempel, Astrophys. J. **762**, L22 (2013) [arXiv:1207.4466 [astro-ph.HE]].
- [6] M. Su and D. P. Finkbeiner, arXiv:1207.7060 [astro-ph.HE].
- [7] D. Hooper and T. Linden, Phys. Rev. D **86**, 083532 (2012) [arXiv:1208.0828 [astro-ph.HE]].
- [8] D. P. Finkbeiner, M. Su and C. Weniger, JCAP **1301**, 029 (2013) [arXiv:1209.4562 [astro-ph.HE]].
- [9] A. Boyarsky, D. Malyshev and O. Ruchayskiy, Phys. Dark Univ. **2**, 90 (2013) [arXiv:1205.4700 [astro-ph.HE]].

- [10] D. Whiteson, JCAP **1211**, 008 (2012) [arXiv:1208.3677 [astro-ph.HE]].
- [11] A. Hektor, M. Raidal and E. Tempel, arXiv:1209.4548 [astro-ph.HE].
- [12] N. Mirabal, Mon. Not. Roy. Astron. Soc. **429**, L109 (2013) [arXiv:1208.1693 [astro-ph.HE]].
- [13] C. Weniger, M. Su, D. P. Finkbeiner, T. Bringmann and N. Mirabal, arXiv:1305.4710 [astro-ph.HE].
- [14] [Fermi-LAT Collaboration], Physical Review D **88**, **082002** (2013) [arXiv:1305.5597 [astro-ph.HE]].
- [15] J. M. Cline, Phys. Rev. D **86**, 015016 (2012) [arXiv:1205.2688 [hep-ph]], M. R. Buckley and D. Hooper, Phys. Rev. D **86**, 043524 (2012) [arXiv:1205.6811 [hep-ph]].
- [16] E. Dudas, Y. Mambrini, S. Pokorski and A. Romagnoni, JHEP **1210**, 123 (2012) [arXiv:1205.1520 [hep-ph]], K. -Y. Choi and O. Seto, Phys. Rev. D **86**, 043515 (2012) [Erratum-ibid. D **86**, 089904 (2012)] [arXiv:1205.3276 [hep-ph]], B. Kyae and J. -C. Park, arXiv:1205.4151 [hep-ph], H. M. Lee, M. Park and W. -I. Park, Phys. Rev. D **86**, 103502 (2012) [arXiv:1205.4675 [hep-ph]], D. Das, U. Ellwanger and P. Mitropoulos, JCAP **1208**, 003 (2012) [arXiv:1206.2639 [hep-ph]], Z. Kang, T. Li, J. Li and Y. Liu, arXiv:1206.2863 [hep-ph], J. -C. Park and S. C. Park, Phys. Lett. B **718**, 1401 (2013) [arXiv:1207.4981 [hep-ph]], Y. Bai and J. Shelton, JHEP **1212**, 056 (2012) [arXiv:1208.4100 [hep-ph]], L. Wang and X. -F. Han, Phys. Rev. D **87**, 015015 (2013) [arXiv:1209.0376 [hep-ph]], K. Schmidt-Hoberg, F. Staub and M. W. Winkler, JHEP **1301**, 124 (2013) [arXiv:1211.2835 [hep-ph]], G. Chalons, M. J. Dolan and C. McCabe, arXiv:1211.5154 [hep-ph].
- [17] W. Buchmuller and M. Garny, JCAP **1208**, 035 (2012) [arXiv:1206.7056 [hep-ph]].
- [18] N. Jarosik, C. L. Bennett, J. Dunkley, B. Gold, M. R. Greason, M. Halpern, R. S. Hill and G. Hinshaw *et al.*, Astrophys. J. Suppl. **192**, 14 (2011) [arXiv:1001.4744 [astro-ph.CO]].
- [19] V. Silveira and A. Zee, Phys. Lett. B **161**, 136 (1985), J. McDonald, Phys. Rev. D **50**, 3637 (1994) [hep-ph/0702143 [HEP-PH]], C. P. Burgess, M. Pospelov and T. ter Veldhuis, M. C. Bento, O. Bertolami, R. Rosenfeld and L. Teodoro, Phys. Rev. D **62**, 041302 (2000) [astro-ph/0003350], Nucl. Phys. B **619**, 709 (2001) [hep-ph/0011335], V. Barger, P. Langacker, M. McCaskey, M. J. Ramsey-Musolf and G. Shaughnessy, Phys. Rev. D **77**, 035005 (2008) [arXiv:0706.4311 [hep-ph]], S. Andreas, T. Hambye and M. H. G. Tytgat, JCAP **0810**, 034 (2008) [arXiv:0808.0255 [hep-ph]], C. E. Yaguna, JCAP **0903**, 003 (2009) [arXiv:0810.4267 [hep-ph]], X. -G. He, T. Li, X. -Q. Li, J. Tandean and H. -C. Tsai,



- Phys. Rev. D **79**, 023521 (2009) [arXiv:0811.0658 [hep-ph]], X. -G. He, T. Li, X. -Q. Li, J. Tandean and H. -C. Tsai, Phys. Lett. B **688**, 332 (2010) [arXiv:0912.4722 [hep-ph]], A. Bandyopadhyay, S. Chakraborty, A. Ghosal and D. Majumdar, JHEP **1011**, 065 (2010) [arXiv:1003.0809 [hep-ph]], S. Andreas, C. Arina, T. Hambye, F. -S. Ling and M. H. G. Tytgat, Phys. Rev. D **82**, 043522 (2010) [arXiv:1003.2595 [hep-ph]], Y. Mambrini, Phys. Rev. D **84**, 115017 (2011) [arXiv:1108.0671 [hep-ph]].
- [20] S. Profumo, L. Ubaldi and C. Wainwright, Phys. Rev. D **82**, 123514 (2010) [arXiv:1009.5377 [hep-ph]].
- [21] A. Biswas and D. Majumdar, Pramana **80**, 539 (2013) [arXiv:1102.3024 [hep-ph]].
- [22] S. Chatrchyan *et al.* [CMS Collaboration], Phys. Lett. B **716**, 30 (2012) [arXiv:1207.7235 [hep-ex]], G. Aad *et al.* [ATLAS Collaboration], Phys. Lett. B **716**, 1 (2012) [arXiv:1207.7214 [hep-ex]].
- [23] E. Ma, Phys. Rev. D **73**, 077301 (2006) [hep-ph/0601225], L. Lopez Honorez, E. Nezri, J. F. Oliver and M. H. G. Tytgat, JCAP **0702**, 028 (2007) [hep-ph/0612275], D. Majumdar and A. Ghosal, Mod. Phys. Lett. A **23**, 2011 (2008) [hep-ph/0607067], M. Gustafsson, E. Lundstrom, L. Bergstrom and J. Edsjo, Phys. Rev. Lett. **99**, 041301 (2007) [astro-ph/0703512 [ASTRO-PH]], Q. -H. Cao, E. Ma and G. Rajasekaran, Phys. Rev. D **76**, 095011 (2007) [arXiv:0708.2939 [hep-ph]], E. Lundstrom, M. Gustafsson and J. Edsjo, Phys. Rev. D **79**, 035013 (2009) [arXiv:0810.3924 [hep-ph]], E. Nezri, M. H. G. Tytgat and G. Ver-tongen, JCAP **0904**, 014 (2009) [arXiv:0901.2556 [hep-ph]], S. Andreas, M. H. G. Tytgat and Q. Swillens, JCAP **0904**, 004 (2009) [arXiv:0901.1750 [hep-ph]], C. Arina, F. -S. Ling and M. H. G. Tytgat, JCAP **0910**, 018 (2009) [arXiv:0907.0430 [hep-ph]], L. Lopez Honorez and C. E. Yaguna, JHEP **1009**, 046 (2010) [arXiv:1003.3125 [hep-ph]], D. Borah and J. M. Cline, Phys. Rev. D **86**, 055001 (2012) [arXiv:1204.4722 [hep-ph]].
- [24] L. Lopez Honorez and C. E. Yaguna, JCAP **1101**, 002 (2011) [arXiv:1011.1411 [hep-ph]].
- [25] R. Barbieri, L. J. Hall and V. S. Rychkov, Phys. Rev. D **74**, 015007 (2006) [hep-ph/0603188].
- [26] M. Kadastik, K. Kannike and M. Raidal, Phys. Rev. D **81**, 015002 (2010) [arXiv:0903.2475 [hep-ph]].
- [27] M. Kadastik, K. Kannike and M. Raidal, Phys. Rev. D **80**, 085020 (2009) [Erratum-ibid. D **81**, 029903 (2010)] [arXiv:0907.1894 [hep-ph]].
- [28] Q. -H. Cao, E. Ma, J. Wudka and C. -P. Yuan, arXiv:0711.3881 [hep-ph].

- [29] J. F. Navarro, C. S. Frenk and S. D. M. White, *Astrophys. J.* **490**, 493 (1997) [astro-ph/9611107].
- [30] J. Einasto, *Trudy Inst. Astrofiz. Alma-Ata* **5** (1965) 87, J. F. Navarro *et al.*, *Mon. Not. Roy. Astron. Soc.* **349**, 1039 (2004); astro-ph/0311231.
- [31] G. Abbiendi *et al.* [OPAL Collaboration], *Eur. Phys. J. C* **19**, 587 (2001) [hep-ex/0012018].
- [32] R. Barbieri, M. Frigeni and G. F. Giudice, *Nucl. Phys. B* **313**, 725 (1989).
- [33] A. Melfo, M. Nemevsek, F. Nesti, G. Senjanovic and Y. Zhang, *Phys. Rev. D* **84** (2011) 034009 [arXiv:1105.4611 [hep-ph]].
- [34] Y. Mambrini, *Phys. Rev. D* **84** (2011) 115017 [arXiv:1108.0671 [hep-ph]], J. Giedt, A. W. Thomas and R. D. Young, *Phys. Rev. Lett.* **103** (2009) 201802 [arXiv:0907.4177 [hep-ph]].
- [35] E. Aprile *et al.* [XENON100 Collaboration], *Phys. Rev. Lett.* **109**, 181301 (2012) [arXiv:1207.5988 [astro-ph.CO]].
- [36] G. Belanger and J. -C. Park, *JCAP* **1203**, 038 (2012) [arXiv:1112.4491 [hep-ph]].
- [37] J. Edsjo and P. Gondolo, *Phys. Rev. D* **56**, 1879 (1997) [hep-ph/9704361].
- [38] W-L. Guo and Y-L. Wu, *JHEP* **1010** (2010) 083 [arXiv:1006.2518 [hep-ph]].
- [39] K. Griest and D. Seckel, *Phys. Rev. D* **43**, 3191 (1991).
- [40] G. Abbiendi *et al.* [ALEPH and DELPHI and L3 and OPAL and The LEP working group for Higgs boson searches Collaborations], [arXiv:1301.6065 [hep-ex]].
- [41] M. Cirelli, G. Corcella, A. Hektor, G. Hutsi, M. Kadastik, P. Panci, M. Raidal and F. Sala *et al.*, *JCAP* **1103**, 051 (2011) [Erratum-ibid. **1210**, E01 (2012)] [arXiv:1012.4515 [hep-ph]].
- [42] R. Catena and P. Ullio, *JCAP* **1008**, 004 (2010) [arXiv:0907.0018 [astro-ph.CO]], P. Salucci, F. Nesti, G. Gentile and C. F. Martins, *Astron. Astrophys.* **523**, A83 (2010) [arXiv:1003.3101 [astro-ph.GA]].
- [43] M. Ackermann *et al.* [LAT Collaboration], *Phys. Rev. D* **86**, 022002 (2012) [arXiv:1205.2739 [astro-ph.HE]].

- [44] T. Yamagata, Y. Takamori and H. Utsunomiya, Phys. Rev. D **47**, 1231 (1993); C. F. Berger, L. Covi, S. Kraml and F. Palorini, JCAP **0810**, 005 (2008) [arXiv:0807.0211 [hep-ph]]; L. Chuzhoy and E. W. Kolb, JCAP **0907**, 014 (2009) [arXiv:0809.0436 [astro-ph]].
  - [45] P. Osland, A. Pukhov, G. M. Pruna and M. Purmohammadi, JHEP **1304**, 040 (2013) [arXiv:1302.3713 [hep-ph]].
  - [46] Z. Ahmed *et al.* [CDMS-II Collaboration], Science **327**, 1619 (2010) [arXiv:0912.3592 [astro-ph.CO]].
  - [47] E. Armengaud *et al.* [EDELWEISS Collaboration], Phys. Lett. B **702**, 329 (2011) [arXiv:1103.4070 [astro-ph.CO]].
  - [48] P. M. Ferreira and D. R. T. Jones, JHEP **0908**, 069 (2009) [arXiv:0903.2856 [hep-ph]], A. Goudelis, B. Herrmann and O. Stl, arXiv:1303.3010 [hep-ph].
-